

1 **Characterization of biogenic volatile organic compounds and their**
2 **oxidation products at a stressed spruce-dominated forest close to a**
3 **biogas power plant**

4
5 Junwei Song^{1,4,*}, Georgios I. Gkatzelis², Ralf Tillmann², Nicolas Brüggemann³, Thomas
6 Leisner¹ and Harald Saathoff^{1,*}

7 ¹ Institute of Meteorology and Climate Research, Karlsruhe Institute of Technology,
8 Hermann-von-Helmholtz-Platz 1, 76344 Eggenstein-Leopoldshafen, Germany

9 ² Institute of Energy and Climate Research, IEK-8: Troposphere, Forschungszentrum
10 Jülich GmbH, 52425 Jülich, Germany

11 ³ Institute of Bio- and Geosciences, IBG-3: Agrosphere, Forschungszentrum Jülich GmbH,
12 52425 Jülich, Germany

13 ⁴ Université Claude Bernard Lyon 1, CNRS, IRCELYON, UMR 5256, F-69626,
14 Villeurbanne, France

15
16 Correspondence: Junwei Song (junwei.song@ircelyon.univ-lyon1.fr) and Harald Saathoff
17 (harald.saathoff@kit.edu)

18 **Abstract**

19 Biogenic volatile organic compounds (BVOCs) are key components of the atmosphere, playing
20 a significant role in the formation of organic aerosols (OA). However, only few studies have
21 simultaneously examined the characteristics of BVOCs and OA in the forest under the impact
22 of consecutive droughts and extensive bark beetle infestations. Here we present real-time
23 measurements of OA and BVOCs at a stressed spruce-dominated forest near a biogas power
24 plant (BPP) in western Germany during June 2020. A proton-transfer-reaction time-of-flight
25 mass spectrometer coupled with a particle inlet (CHARON-PTR-ToF-MS) and a Vocus-PTR-
26 ToF-MS were used to measure OA and BVOCs. The average mass concentration of OA was
27 $0.8 \pm 0.5 \mu\text{g m}^{-3}$, consisting mainly of semi-volatile monoterpene oxidation products. The
28 average mixing ratios of isoprene (0.58 ± 0.54 ppb) and monoterpenes (2.5 ± 5.3 ppb) were
29 higher than the values previously measured in both German temperate forests and boreal forests.
30 Based on wind direction analysis, BVOC data were categorized into two groups with one
31 mainly influenced by the biogenic emissions from an intact forest and a clear-cut area (biogenic-
32 group) and another one by the anthropogenic emissions from a BPP and a village
33 (anthropogenic-group). High mixing ratios of monoterpenes were observed in the
34 anthropogenic-group, indicating a significant contribution of BPP emissions. In the biogenic-
35 group, the variations of BVOC mixing ratios were driven by the interplay between meteorology,
36 biogenic emissions and their photochemical consumption. Positive matrix factorization analysis
37 of VOCs revealed substantial contributions of oxygenated organic compounds from the
38 photochemical oxidation of BVOCs during daytime, while monoterpenes and their weakly
39 oxidized products dominated at night. Furthermore, increasing relative humidity and decreasing
40 temperatures promoted the gas-to-particle partitioning of these weakly oxidized monoterpene
41 products, leading to an increase in nighttime OA mass. The results demonstrate the variations
42 of BVOCs are influenced not only by meteorological conditions and biogenic emissions but
43 also by local BPP emissions and subsequent chemical transformation processes. This study
44 highlights the need to investigate the changes of biogenic emissions in European stressed
45 forests.

46

47 **1 Introduction**

48 Volatile organic compounds (VOCs) play important roles in determining atmospheric
49 chemical processes (Atkinson, 2000; Hallquist et al., 2009; Yáñez-Serrano et al., 2020;
50 Shrivastava et al., 2017; Rasmussen and Went, 1965; Trainer et al., 1987; Peñuelas and Staudt,

51 2010). Terrestrial ecosystems emit large amounts of biogenic VOCs (BVOCs, >1000 Tg yr⁻¹)
52 to the global atmosphere, more than anthropogenic VOCs (AVOCs, ~200 Tg yr⁻¹) (Guenther et
53 al., 2012; Sindelarova et al., 2014). BVOCs emitted by vegetation consist largely of reactive
54 terpenoids e.g., isoprene (~70%), monoterpenes (~11%) and sesquiterpenes (~2.5%)
55 (Sindelarova et al., 2014). The oxidation products of terpenoids can nucleate to form new
56 particles or contribute to the growth of existing particles and secondary organic aerosol (SOA)
57 formation, thus impacting air quality and climate (Hallquist et al., 2009; Shrivastava et al.,
58 2017).

59 Over the last decade, many field studies have been conducted at different forest ecosystems
60 to investigate the characteristics of BVOCs including the emissions, temporal variations as well
61 as their impacts on atmospheric reactivity and SOA formation (Hakola et al., 2012; Hellén et
62 al., 2018; Li et al., 2020; Huang et al., 2021; Yáñez-Serrano et al., 2021; Vestenius et al., 2021;
63 Mermet et al., 2021; Vermeuel et al., 2023; Weber et al., 2022; Bourtsoukidis et al., 2024;
64 Bourtsoukidis et al., 2014). The diurnal pattern of isoprene concentrations in forests shows
65 typically higher values during daytime (Yáñez-Serrano et al., 2021; Li et al., 2020; Hakola et
66 al., 2012), since isoprene emissions increase with temperature and sunlight intensity as result
67 of increased de-novo production and direct release. In contrast, monoterpenes are mainly
68 released from storage pools of boreal pines. The emissions and composition of BVOCs from
69 trees varies with abiotic and biotic stresses such as high temperature (Teskey et al., 2015; Kleist
70 et al., 2012), drought (Peron et al., 2021; Bonn et al., 2019) and herbivore attack (Jaakkola et
71 al., 2023; Kari et al., 2019; Faiola and Taipale, 2020). It has been reported that these stresses
72 can alter the emissions of BVOCs, especially of terpenoids (Ghimire et al., 2016; Jaakkola et
73 al., 2023; Byron et al., 2022).

74 In addition to biogenic emissions, the temporal variations of BVOC concentrations
75 especially of terpenoids are influenced by atmospheric oxidation processes. The diurnal
76 variation of monoterpene concentrations shows lower values during daytime than nighttime in
77 the boreal forests, which were attributed to the rapid photochemical consumption and expanded
78 boundary layer heights (Hellén et al., 2018; Hakola et al., 2012). Correspondingly, higher
79 concentrations of monoterpene oxidation products are expected to be produced during daytime.
80 For instance, Huang et al., (2021) found that some gaseous monoterpene oxidation products
81 e.g., C₇H₁₀O₄ (3,6-oxoheptanoic acid) and C₈H₁₂O₄ (terpenylic acid) showed higher
82 concentrations during daytime in a boreal forest. Li et al., (2020) reported similar diurnal
83 variations of gaseous higher-oxidized monoterpene products (e.g., C₈H₁₂O₄₋₆, C₉H₁₄O₄₋₆,
84 C₁₀H₁₄O₄₋₆ and C₁₀H₁₆O₄₋₆) in the French Landes-forest largely composed of maritime pines.

85 The variations of BVOC oxidation products are also influenced by gas-particle partitioning
86 processes. Laboratory studies have shown that decreasing temperature and increasing relative
87 humidity (RH) can lead to an increased particulate fraction of SOA products from BVOC
88 oxidation (Surdu et al., 2023; Von Hessberg et al., 2009; Tillmann et al., 2010; Zhang et al.,
89 2015; Luo et al., 2024). However, due to lack of online dual-phase measurements only few field
90 studies have focused on the gas-particle partitioning of BVOC oxidation products in the healthy
91 forests (Mohr et al., 2017; Yatavelli et al., 2014; Isaacman-Vanwertz et al., 2016; Lee et al.,
92 2018). However, our understanding of the interplay between gas and particle phases of BVOC
93 oxidation products in real forest atmosphere, particularly in stressed forest, remains limited.
94 Addressing these gaps is crucial for assessing the impact of various environmental factors on
95 BVOC emissions and their subsequent transformation (Faiola and Taipale, 2020).

96 The Eifel is a low mountain range in western Germany that stretches across the federal states
97 of North Rhine-Westphalia and Rhineland-Palatinate and covers an area of ~5300 km². Its
98 forested areas are largely composed of Norway spruce (*Picea abies* (L.) Karst.), which are
99 important contributors to BVOCs (Smiatek and Steinbrecher, 2006; Kleist et al., 2012). The
100 Eifel Forest was suffering from severe droughts, heatwaves and bark beetle infestation in the
101 years before our measurements, thus it can serve as a case for examining the variations of
102 BVOCs in a stressed European coniferous forest. In this study, a field measurement campaign
103 was conducted at a site of the northern Eifel Forest in the vicinity of a biogas power plant (BPP).
104 Europe is the world leader in biogas electricity production with more than 18,000 BPPs
105 (Brémond et al., 2021). These BPPs are widely distributed in European rural areas close to the
106 forest region (Bakkaloglu et al., 2021; Scheftelowitz et al., 2018), which emit large amounts of
107 CH₄ and VOCs periodically to the atmosphere around the BPPs (Salazar Gómez et al., 2016).
108 In this paper, we present the real-time measurements of VOCs and aerosol particles measured
109 by a proton-transfer-reaction time-of-flight mass spectrometer (PTR-ToF-MS) coupled with a
110 particle inlet (CHARON, chemical analysis of aerosol online) and a Vocus-PTR-ToF-MS. The
111 impacts of meteorological conditions, sources and chemical oxidation processes on the
112 variations of BVOCs and their gaseous and particulate oxidation products were investigated to
113 get a better understanding of BVOC emissions and their contributions to SOA as well as the
114 potential impact of BPP emissions.

115 **2 Methods**

116 **2.1 Sampling site**

117 In this study, a three-week field campaign was conducted at a site in the northern Eifel
118 Forest (50.72° N, 6.40° E) during June 2020 as a part of the “Heat and Drought 2020” campaign
119 of the Modular Observation Solutions of Earth Systems (MOSES) project of the Helmholtz
120 Association of German Research Centers. The Eifel Forest was suffering from severe droughts,
121 heatwaves and severe bark beetle infestation in the last years (Weber et al., 2022b; Ghimire et
122 al., 2016). Within two years (2018-2020), 14% of the spruce in the Northern Eifel region were
123 removed due to summer droughts and only 28.3% remained in good condition (Montzka et al.,
124 2021). Therefore, the Eifel Forest can serve as an example of a stressed temperate coniferous
125 forest.

126 As shown in **Fig. 1**, the measurement site is situated directly next to a stand of Norway
127 spruce with a few shrubs and blueberry plants also surrounding the area. To the south and
128 southeast of the measurements site, there were some clear-cut areas due to bark beetle
129 infestation in the years of 2018-2020. Additionally, the measurement site was located ~400 m
130 southeast of a football field in the small village Kleinhau belonging to the municipality of
131 Hürtgenwald, Germany (population about 9000) and ~250 m east of a BPP (BioEnergie
132 Kleinhau GmbH). The biomass substrate used for the biogas production in this BPP consisted
133 mainly of crop waste (e.g., corn stover). The measurement site was affected by the BPP
134 emissions especially for westerly wind directions.

135 **2.2 Instrumentation**

136 All instruments were set up in a temperature-controlled measurement container (~25 °C)
137 located at the sampling site. All sampling inlets were located 3.7 m above ground level and 1
138 m above the container roof. An overview of instruments and parameters measured is given in
139 **Table S1**.

140 A PTR-ToF-MS 4000X2 coupled with a CHARON particle inlet (Ionicon Analytik GmbH,
141 Innsbruck, Austria) was deployed to measure the VOCs and aerosol particles from 5th-30th of
142 June 2020. A detailed description of the PTR-ToF-MS and CHARON inlet has been provided
143 elsewhere (Jordan et al., 2009; Muller et al., 2017; Eichler et al., 2015). Briefly, CHARON
144 consists of a charcoal denuder for stripping off gaseous organics, an aerodynamic lens for
145 enriching particles, and a thermo-desorption unit for particle evaporation prior to chemical
146 analysis by PTR-ToF-MS. In this campaign, both gases and particles were measured through
147 alternatingly switching between different modes with the data acquisition software (IoniTOF

148 4.0, Ionicon Analytik GmbH, Innsbruck, Austria). Specifically, one alternating measurement
149 cycle includes 3-min HEPA filter mode for measuring the particle background, 1-min transition
150 mode for the instrument equilibrium, 10-min CHARON mode for measuring particle phase
151 compounds, another 1-min transition mode and 10-min VOC mode for measuring gas phase
152 compounds (**Fig. S1**). One minute transition time is sufficient for the equilibrium of
153 instrumental conditions between different modes (Piel et al., 2021). During the gas-phase
154 measurement, ambient air was sampled continuously from a 3 m long perfluoroalkoxy tube (1/4
155 inch inner diameter) with a total flowrate of 1.45 L min⁻¹, and then a subset flow of ~0.1 L min⁻¹
156 was sampled by the PTR-MS through a polyetheretherketone tubing maintained at 80 °C.
157 During the particle-phase measurement, ambient particles were sampled by a PM_{2.5} inlet with a
158 flowrate of 16.7 L min⁻¹, out of which a flow of 0.55 L min⁻¹ was directed to the CHARON
159 inlet maintained by a vacuum pump (ACP15, Pfeiffer Vacuum). During a first measurement
160 stage from 5th-19th of June, the PTR drift tube was set with alternating temperatures for gas and
161 particle phase measurement modes at 80 °C and 120 °C respectively. With this setting, the
162 actual drift tube temperatures were varying during the gas and particle measurement modes
163 complicating the data analysis (**Figs. S1 and S2**). During a second measurement stage from
164 22nd-30th of June, the PTR drift tube was set with the same temperature of 120 °C and a drift
165 tube pressure of 2.7 mbar for both gas and particle measurement modes. The CHARON inlet
166 was set to a thermo-desorption unit temperature of 150 °C and a pressure of 7-8 mbar. Finally,
167 the electric field (E/N) of the CHARON-PTR-TOF-MS was kept at ~97 Td and ~57 Td for the
168 gas and particle phase measurement modes respectively during the second measurement stage.
169 Please note that during the first measurement stage the actual temperature of the drift tube
170 fluctuated and was lower than the intended temperature of 120 °C (**Fig. S1**). This made it
171 difficult to quantify organic compounds in the particle phase measured by the CHARON-PTR-
172 ToF-MS. For the gas phase measurements, we corrected the major VOC data from the first
173 measurement stage based on the gas calibration and the cross-comparison with Vocus-PTR-
174 ToF-MS measurements. Consequently, we can present the major VOC species measured by the
175 CHARON-PTR-ToF-MS for the entire campaign, while the particle phase data for first
176 measurement stage were excluded for further analysis in this study.

177 Gas calibrations of CHARON-PTR-ToF-MS were performed via dynamic dilution of a
178 calibration gas cylinder containing 11 VOC species (**Table S2**, accuracy 10% at ~100 ppb).
179 The background of VOCs was taken from zero-air measurements during the gas calibrations at
180 the beginning and the end of the campaign. The enrichment factor of the CHARON inlet was
181 determined using an external calibration with size-selected ammonium nitrate particles

182 (NH₄NO₃) that were counted using a condensation particle counter (CPC3772, TSI Inc.,
183 Shoreview, MN, USA). The enrichment factor was determined with an average value of 18 ± 2
184 in the 150-700 nm particle size range, with lower values for smaller particles below 150 nm
185 (**Fig. S3**). The particle background was determined by a high-efficiency HEPA filter (ETA filter
186 model HC01-5N-B, Aerocolloid LLC, Minneapolis, MN, USA) that was placed upstream of
187 the gas-phase denuder of the CHARON inlet. All data files recorded by the CHARON-PTR-
188 ToF-MS were processed by the software IONICON Data Analyzer (IDA version 1.0.0.2,
189 Ionicon Analytik GmbH, Innsbruck, Austria). More details of data processing with the IDA are
190 given in **Supplement S1**.

191 A Vocus-PTR-ToF-MS (Aerodyne Research Inc., Billerica, MA, USA) was deployed to
192 measure VOCs and oxygenated VOCs concurrently with the CHARON-PTR-ToF-MS from
193 10th-30th of June. The Vocus-PTR-ToF-MS was not available for measurements before 10th June
194 2020 due to a technical problem. The details of the Vocus-PTR-ToF-MS have been described
195 elsewhere (Krechmer et al., 2018). The Vocus-PTR-ToF-MS is characterized by a newly
196 designed reagent-ion source and a focusing ion-molecule reactor (FIMR), both of which
197 improve the detection efficiency of ions. In this study, the FIMR was operated at a pressure of
198 1.5 mbar. The mass resolving power of the Vocus mass analyzer was ~ 10000 amu/ Δ amu. Raw
199 data were recorded with a time resolution of 5 s. For the Vocus-PTR-ToF-MS measurement,
200 ambient air was drawn in through a 1 m long PFA tubing with a total flow rate of 4.5 L min^{-1} ,
201 and then a subset flow of $0.1\text{-}0.15 \text{ L min}^{-1}$ went into the Vocus-PTR-ToF-MS. Background
202 measurements using high-purity nitrogen were automatically performed every hour. The
203 Vocus-PTR-ToF-MS was regularly calibrated using a home-made gas standard of 15
204 compounds at ~ 1 ppmv with accuracy of 10% (**Table S2**). At the end of the campaign, a gas
205 cross calibration was performed between Vocus-PTR-ToF-MS and CHARON-PTR-ToF-MS
206 with the calibration gas cylinder (Ionicon Analytik GmbH). The Vocus-PTR-ToF-MS data
207 analysis was performed using the software package “TOFware” (AG, Thun, Switzerland). For
208 the quantification of uncalibrated species measured by the Vocus-PTR-ToF-MS, we adopted
209 the rate constants of proton transfer reactions (K_{cap}) from the PTR library (Pagonis et al., 2019).
210 We then generated a sensitivity for the uncalibrated masses by applying a correction factor
211 based on the k_{cap} ratios to the calibrated masses. Finally, the Vocus-PTR-ToF-MS data were
212 synchronized to the measurement time of CHARON-PTR-ToF-MS for comparison of the VOC
213 data. In this study, a series of VOC species were simultaneously detected by the CHARON-
214 PTR-ToF-MS and the Vocus-PTR-ToF-MS with a detailed comparison provided in
215 **Supplement S2**.

216 In addition, methane (CH₄), carbon dioxide (CO₂), water vapor (H₂O) and carbon monoxide
217 (CO) were measured with a cavity ring-down spectrometer (G2401; Picarro, Santa Clara, CA,
218 USA) from 10th-30th of June. O₃ was measured by a commercial chemiluminescence analyzer
219 (Cranox II, Eco Physics GmbH, Hürth, Germany). An optical particle counter (OPC, Fidas200,
220 Palas, Karlsruhe, Germany) was used to measure the mass concentrations of PM_{2.5} and PM₁₀
221 from 5th-30th of June. Simultaneously, black carbon (BC) concentrations were measured with
222 an aethalometer (MA200, AethLabs, CA, USA). Particle number concentrations were measured
223 with a condensation particle counter (CPC3776, TSI Inc., Shoreview, MN, USA). A
224 nanoparticle sizer (NanoScan SMPS, TSI3910, TSI Inc., Shoreview, MN, USA) was used to
225 measure the particle number size distribution between 10-410 nm.

226 Meteorological parameters were measured by a compact sensor (WS700, Lufft GmbH,
227 Fellbach, Germany). The meteorological data were missing during some short periods due to
228 the malfunction of data acquisition. We also used hourly data of temperature, relative humidity,
229 precipitation, and planetary boundary layer (PBL) height from the European Centre for
230 Medium-Range Weather Forecasts ERA5 reanalysis (Hersbach et al., 2020), as well as wind
231 speed and direction data from NASA Power Data Access Viewer (power.larc.nasa.gov) to
232 complement the meteorological data. The daily soil moisture was measured by a Cosmic-Ray
233 Neutron Sensor (CRNS) (Bogena et al., 2015), which was located ~150 m southwest of the
234 sampling site. In addition, the spatial distribution of soil moisture in the northern Eifel Forest
235 was determined from the measurement of a CRNS rover.

236 **2.3 Positive matrix factorization analysis**

237 The PMF receptor model is a bilinear analytic algorithm that separates the time series of air
238 pollutants to different sources represented by factor profiles, factor time series and residual
239 signals (Paatero and Tapper, 1994). The PMF model has been widely used to determine
240 different sources and chemical processes of VOCs measured by the PTR-ToF-MS in the urban,
241 rural and forest atmospheres (Gkatzelis et al., 2021; Li et al., 2021a; Wang et al., 2020; Li et
242 al., 2022; Pernov et al., 2021; Desservettaz et al., 2023; Jain et al., 2023; Song et al., 2024). To
243 explore the sources and chemical processes of VOCs, we performed the PMF analysis of VOC
244 species measured by the Vocus-PTR-ToF-MS rather than those measured by CHARON-PTR-
245 ToF-MS. This is mainly due to the Vocus-PTR-ToF-MS can measure higher molecular weight
246 OVOCs ($m_z > 200$) well that provides more information for interpreting the oxidation processes
247 of BVOCs (Li et al., 2021a).

248 In this study, the Vocus-PTR-ToF-MS-measured VOC ions with a chemical formula
249 assignment (mainly $C_xH_y^+$ and $C_xH_yO_z^+$) were selected to perform the PMF analysis. The PMF
250 input data was prepared according to the protocol reported in previous studies (Pernov et al.,
251 2021; Li et al., 2022). The uncertainties were calculated with the following equations:

$$252 \quad Unc. = \begin{cases} LOD \times \frac{5}{6} & conc \leq LOD \quad (1) \\ \sqrt{LOD^2 + (Error\ fraction \times conc.)^2} & conc. > LOD \quad (2) \end{cases}$$

253 where the concentrations of a VOC ion below the limit of detection (LOD) were replaced with
254 half of the LOD and the associated uncertainties were set to 5/6 of the LOD using the equation
255 1. The uncertainties of a VOC ion above the LOD were calculated using the equation 2,
256 assuming an error fraction of 10%. We excluded the VOC species from the PMF analysis if
257 their concentration data are significantly below LOD (> 20%) during the entire measurement
258 campaign. For example, we excluded the signal of $C_4H_9^+$ for PMF analysis because its signals
259 were mostly below the LOD during a significant fraction of the measurement period (**Fig. S4**).
260 Finally, 157 VOC ions were selected for the PMF analysis (**Table S3**). The sum mixing ratios
261 of these 157 VOC ions measured by the Vocus-PTR-ToF-MS showed a good agreement with
262 the sum mixing ratios of 112 major VOC ions simultaneously measured by the CHARON-PTR-
263 ToF-MS (**Fig. S4**). Therefore, the solution of PMF analysis on these 157 VOC ions measured
264 by the Vocus-PTR-ToF-MS can reasonably interpret the major sources and/or chemical
265 processes of VOCs in this study. The PMF analysis was performed using the PMF Evaluation
266 Tool (v3.05) that runs in IGOR Pro software (v6.37, Wavemetrics, Portland, OR). The optimal
267 PMF solution was explored across several solution diagnostics of factors ranging 1 to 10. The
268 6-factor solution was chosen as the optimal and interpretable solution. After 6 factors,
269 increasing the factor number will cause the factor splitting and provide uninterpretable results
270 (**Fig. S5**). The summary of diagnostic plots for the 6-factor solution is given in **Fig. S6**.

271 2.4 Calculation of particle-phase fraction of organic compounds

272 To estimate the gas-to-particle partitioning processes, we calculated the particulate mass
273 fraction (F_p) of organic compounds by the Equation 3:

$$274 \quad F_p = \frac{C_{p,i}}{C_{g,i} + C_{p,i}} \quad (3)$$

275 where $C_{p,i}$ and $C_{g,i}$ are the particle and gas phase concentrations of the individual organic
276 compound measured by CHARON-PTR-ToF-MS and Vocus-PTR-ToF-MS, respectively.

277 **3 Results and discussion**

278 In the first section we will give an overview of the measurements conducted and in the
279 second section we will address the impacts of meteorological factors like wind speed and
280 direction, temperature, and relative humidity on the variations of gas and particle
281 concentrations. In the third section we perform a source apportionment of the VOCs observed,
282 and in the last section we discuss BVOC oxidation products in gas and particle phase.

283 **3.1 Overview of the measurements**

284 **3.1.1 Meteorology**

285 During the entire measurement campaign, the ambient temperature ranged from 6.8 to 30.8
286 °C with an average of 16.6 ± 4.7 °C, and the relative humidity (RH) varied from 31% to 98%
287 with an average of $71\% \pm 16\%$ respectively (**Fig. 2**). The wind speeds ranged from 0-5.5 m s⁻¹
288 with an average of 1.3 ± 0.9 m s⁻¹. Wind directions varied significantly during the entire
289 measurement period. The sampling site was potentially affected by BPP-related and/or
290 anthropogenic emissions depending on the wind directions (**Fig. 1**). The leaf area index of the
291 Eifel Forest during our measurement period was determined to be $\sim 2.5 \pm 0.02$ m² m⁻² based on
292 the ERA5 reanalysis data. The soil moisture was measured to be 0.3 ± 0.04 m³ m⁻³ at a station
293 located ~ 150 m southwest of the sampling site. In addition, the spatial distribution of soil
294 moisture in the northern Eifel Forest also showed low values (< 0.3 m³ m⁻³) in most areas
295 covering our sampling site (**Fig. S7**). Therefore, the Eifel Forest was under relatively dry
296 condition during our measurement period.

297 During the entire measurement campaign, we observed two characteristic episodes, Episode
298 1 (0:00 9th of June to 0:00 12th of June) and Episode 2 (12:00 23rd of June to 12:00 26th of June),
299 for different meteorological conditions. During Episode 1, the daily maximum temperature
300 remained below 20 °C for three consecutive measurement days. During Episode 2, the daily
301 maximum temperature exceeded 25 °C for three consecutive measurement days. Therefore,
302 hereafter we define these two episodes as low-T and high-T episodes, respectively. Both
303 episodes had very low wind speeds (< 1 m s⁻¹), suggesting the site was influenced by local
304 emissions and chemical transformation or aging processes. The impacts of meteorology and
305 chemical processes on the variations of gases and particles will be discussed in the following
306 sections.

307 3.1.2 Mixing ratios of gas species

308 As shown in **Fig. 3**, the average mixing ratios of CO and CO₂ were 0.11 ± 0.02 ppm and
309 410 ± 1 ppm respectively from 10th-30th of June. The mixing ratios of CH₄ ranged from 1.90 to
310 2.56 ppm with an average of 1.98 ± 0.05 ppm. Spikes of CH₄ (> 2.2 ppm) were occasionally
311 observed during the days of 17, 20-21 and 23 June, which are associated with BPP-related
312 emissions as validated in Section 3.2. Isoprene and monoterpenes were quantitatively measured
313 by the CHARON-PTR-ToF-MS and Vocus-PTR-ToF-MS with good to fair correlations ($r =$
314 0.92 and 0.59 for isoprene and monoterpenes, respectively). During the entire campaign, the
315 average mixing ratios of isoprene was 0.58 ± 0.54 ppb, slightly higher than that previously
316 reported in a Norway spruce-dominated forest (0.32 ± 0.17 ppb) in central Germany
317 (Bourtsoukidis et al., 2014) and a mixed-conifer forest (max. 0.25 ppb) with Norway spruce
318 and Scots pine (*Pinus sylvestris* L.) in Sweden (Petersen et al., 2023). The level of isoprene in
319 this study was comparable to that (~ 0.6 ppb) observed in French Landes forest dominated by
320 maritime pine trees (*Pinus pinaster* Aiton) during summer time (Li et al., 2020), but higher than
321 those (0.01-0.2 ppb) reported for the boreal forests in Finland dominated by Scots pine (Li et
322 al., 2021a; Hellén et al., 2018). The average mixing ratios of monoterpenes (2.5 ± 5.3 ppb) in
323 this study was also higher than that reported in a Norway spruce-dominated forest (0.50 ± 0.21
324 ppb) in central Germany (Bourtsoukidis et al., 2014), but lower than that observed in the French
325 Landes forest (~ 6 ppb) (Li et al., 2020). Relatively low mixing ratios of monoterpenes were
326 reported previously for the boreal forests in Finland (~ 0.8 ppb) during summertime (Li et al.,
327 2020; Mermet et al., 2021). Note that monoterpenes had a significant concentration variation in
328 this study, which was attributed to the occurrence of monoterpene spikes (**Fig. 3d**). These
329 monoterpene spikes were mainly related to the impact of BPP-related emissions as discussed in
330 section 3.2. In this study, the average mixing ratios of sesquiterpenes measured by the
331 CHARON-PTR-ToF-MS was 0.01 ± 0.01 ppb, a factor of two higher than that measured by the
332 Vocus-PTR-ToF-MS. The average mixing ratios of sesquiterpenes was lower than that
333 measured by a Vocus-PTR-ToF-MS in the French Landes forest (~ 0.06 ppb) (Li et al., 2020).
334 It should be noted that the quantification of sesquiterpenes is affected by the degree of
335 sesquiterpene fragmentation inside the PTR-ToF-MS, which can vary significantly depending
336 on the instrument setting (Kim et al., 2009; Kari et al., 2018). In addition, sesquiterpenes may
337 experience wall losses inside the inlet tubing and the instrument, and have low transmissions
338 (Li et al., 2020). Due to a lack of a dedicated sesquiterpene calibration in this study, the
339 quantification of sesquiterpenes measured by the PTR-ToF-MS can be regarded as the lower
340 limit without the consideration of fragmentation.

341 3.1.3 Chemical composition of aerosol particles

342 During the entire campaign, the average mass concentrations of PM_{2.5} and BC were 5.5 ±
343 4.7 μg m⁻³ and 0.2 ± 0.1 μg m⁻³ respectively (**Fig. S8**). The aerosol particle composition
344 including organic aerosol (OA), nitrate, and ammonium measured by the CHARON-PTR-ToF-
345 MS and BC by the aethalometer are simultaneously available from 22nd-30th of June (**Fig. 4**).
346 During this period, the average mass concentrations of OA was 0.8 ± 0.5 μg m⁻³, accounting
347 for 15 ± 6 % of PM_{2.5} mass. The mass fraction of CHARON-PTR-ToF-MS-measured OA in
348 PM_{2.5} was close to that of semi-volatile oxygenated organic aerosol in PM_{2.5} (9%-13%) resolved
349 from the PMF analysis of OA measured by an aerosol mass spectrometer (AMS) in urban and
350 rural environments (Song et al., 2022; Huang et al., 2019). The elemental ratios of OA (O:C
351 and H:C) measured by the CHARON-PTR-ToF-MS were 0.32 ± 0.03 and 1.56 ± 0.10,
352 respectively, which are comparable to the values of semi-volatile oxygenated organic aerosol
353 (O:C: 0.35 ± 0.14 and H:C: 1.55 ± 0.10) resolved from the AMS-PMF analysis in previous
354 studies (Ng et al., 2011; Ng et al., 2010). These results indicate that the OA mass detected by
355 the CHARON-PTR-ToF-MS is mainly composed of semi-volatile organic compounds in this
356 study. Please note that the fragmentation of organic compounds in the CHARON-PTR-ToF-
357 MS may result in low average O:C values of bulk OA compared to those measured by the AMS
358 (Leglise et al., 2019).

359 Mass concentrations of OA associated with individual *m/z* signals detected by the
360 CHARON-PTR-ToF-MS ranged from ~0.1 to ~65 ng m⁻³. In total, 164 organic ions can be well
361 assigned with the chemical formula of C_xH_y⁺ or C_xH_yO_z⁺, contributing to 67 ± 11 % of total OA
362 mass measured by the CHARON-PTR-ToF-MS. Furthermore, the organic ions assigned were
363 mainly distributed in the C₂-C₁₀ range with oxygen atom numbers of 0-5 (**Fig. 4d**). Müller et
364 al., (2017) observed a similar mass distribution of OA measured by the CHARON-PTR-ToF-
365 MS in Valencia, Spain which was associated with the oxidation of abundant monoterpenes
366 emitted from trees. With the same instrument, Gkatzelis et al., (2018) also reported a similar
367 chemical composition of OA from the oxidation of tree emissions dominated by α-pinene and
368 β-pinene in simulation chamber experiments. The abundant species in the C₂-C₈ range (**Fig. 4d**)
369 are most likely fragments from C₉₋₁₀-monoterpene derived oxidized products which are prone
370 to fragmentation in the CHARON-PTR-ToF-MS (Gkatzelis et al., 2018). Leglise et al., (2019)
371 and Peng et al., (2023) further confirm the fragmentation of oxygenated organic compounds
372 inside the CHARON-PTR-ToF-MS via the loss of neutral water, carbonyl, or carboxyl groups
373 (-H₂O, -CO and -CO₂). For instance, *cis*-pinonic acid (C₁₀H₁₇O₃⁺) a monoterpene oxidation

374 product as detected by the CHARON-PTR-ToF-MS can produce the typical fragment ions of
375 $C_4H_7O^+$, $C_6H_{11}O_2^+$ and $C_{10}H_{15}O_2^+$ (Peng et al., 2023; Leglise et al., 2019). Furthermore, the
376 relative abundance of fragment ions ($C_4H_7O^+$, $C_6H_{11}O_2^+$ and $C_{10}H_{15}O_2^+$) were generally higher
377 than the parent ion $C_{10}H_{17}O_3^+$ (Leglise et al., 2019; Peng et al., 2023). In this study, we found
378 that only a small fraction of the *cis*-pinonic acid parent ion $C_{10}H_{17}O_3^+$ was detected by the
379 CHARON-PTR-ToF-MS compared to the fragment ions $C_4H_7O^+$, $C_6H_{11}O_2^+$ and $C_{10}H_{15}O_2^+$.
380 Similarly, other monoterpene oxidation products such as $C_9H_{15}O_3^+$ (e.g., norpinonic acid) and
381 $C_8H_{13}O_4^+$ (e.g., norpinic acid) showed lower abundances at their parent ions compared to their
382 fragment ions with one H_2O molecule lost ($C_9H_{13}O_2^+$ and $C_8H_{11}O_3^+$) (**Fig. S9**). We observed
383 good correlations between $C_9H_{15}O_3^+$ and $C_9H_{13}O_2^+$ ($r = 0.73$), as well as between $C_8H_{13}O_4^+$ and
384 $C_8H_{11}O_3^+$ ($r = 0.97$), indicating that $C_9H_{13}O_2^+$ and $C_8H_{11}O_3^+$ are fragment ions from parent
385 compounds. Previous studies have shown that the fragmentation pattern of oxidized organic
386 compounds in the CHARON-PTR-ToF-MS varied depending on the instrument settings
387 (Leglise et al., 2019; Gkatzelis et al., 2018). Therefore, we cannot compare the fragmentation
388 patterns of organic compounds from our instruments with those from other studies. However,
389 it is consistent with other studies that the particulate oxidized organic compounds measured by
390 the CHARON-PTR-ToF-MS in this study were mainly detected as the more abundant fragment
391 ions after losing one H_2O molecule rather than as the parent ions.

392 **3.2 Meteorological impacts on the variations of BVOCs**

393 We firstly analyzed the variations in the mixing ratios of gas species as a function of wind
394 direction (WD) with a bin of 10° (**Fig. 5**). According to the wind and geographical conditions
395 around the sampling site (**Fig. 1b**), we divided the entire measurement period into four WD
396 sectors including WD-forest ($0-120^\circ$), WD-cut ($120-240^\circ$), WD-BPP ($240-300^\circ$) and WD-
397 village ($300-330^\circ$). Within the sectors of WD-forest and WD-cut, the sampling site was
398 influenced by an intact forest dominated by Norway spruce and a clear-cut area, respectively.
399 In contrast, the sampling site was influenced by the winds coming from the BPP and the village
400 residential areas within the sectors of WD-BPP and WD-village, respectively. We observed that
401 the mixing ratios of CH_4 increased significantly in the WD-BPP along with the decrease of
402 wind speeds and PBL heights and corresponding weaker dilution. In contrast, constantly low
403 mixing ratios of CH_4 were observed in the WD-forest and WD-cut even when both wind speeds
404 and PBL decreased significantly. The results indicate that the enhancement in CH_4 mixing ratios
405 in the WD-BPP was mainly attributed to the BPP emissions. In addition, CH_4 mixing ratios
406 remained higher for WD-village, which was likely associated with the anthropogenic emissions

407 from the village residential areas. We also observed a significant increase of monoterpene
408 mixing ratios in the WD-BPP along with lower ambient temperature (~15 °C) and decreasing
409 radiation. This suggests that the increase of monoterpene mixing ratios in the WD-BPP was due
410 to BPP emissions rather than biogenic emissions. In contrast to CH₄, monoterpenes showed
411 very low values in the WD-village, suggesting a minor contribution of anthropogenic emissions
412 from the village residential areas to monoterpenes.

413 We also observed significant variations in the mixing ratios of isoprene, monoterpene and
414 sesquiterpene in the WD-forest and WD-cut, likely associated with changes in meteorological
415 conditions, biogenic emissions and/or chemical oxidation processes. Specifically, the mixing
416 ratios of monoterpenes and sesquiterpenes increased in the WD-forest of 0-30° but isoprene
417 showed no significant change. The meteorological condition in the WD-forest of 0-30° was
418 characterized by low ambient temperature, low wind speed and shallow PBL during nighttime.
419 Unlike isoprene, monoterpenes and sesquiterpenes can still be released from the Norway spruce
420 in the dark (Van Meeningen et al., 2017). Monoterpenes and sesquiterpenes could accumulate
421 during nighttime in the WD-forest of 0-30° as a result of low concentrations of atmospheric
422 oxidants like O₃. Besides, we observed an increase of isoprene mixing ratios in the WD-forest
423 of 60-120° which was coincided with the increases of wind speed, PBL, ambient temperature
424 and radiation during daytime. In contrast, monoterpenes and sesquiterpenes showed low mixing
425 ratios in the WD-forest of 60-120°. It is expected that higher temperature and radiation
426 enhanced biogenic emissions, resulting in the increase of isoprene mixing ratios. However,
427 lower mixing ratios of monoterpenes and sesquiterpenes were likely attributed to the
428 photochemical oxidation exceeding their biogenic emissions. The strong photochemical
429 oxidation processes were characterized by higher radiation and O₃ mixing ratios in the WD-
430 forest of 60-120°. In the WD-cut of 120-180°, we observed simultaneous increase of isoprene,
431 monoterpenes and sesquiterpenes, which were associated with enhanced biogenic emissions
432 induced by higher temperature. Conversely, simultaneous decrease of isoprene, monoterpenes
433 and sesquiterpenes mixing ratios were observed in the WD-cut of 180-240° along with high
434 ambient temperature. Note that the sampling site were more influenced by the distant Norway
435 Spruce trees in the WD-cut of 120-180° compared to the WD-cut of 180-240° (**Fig. 1a**). In
436 addition, the wind speeds were significantly higher in the WD-cut of 180-240°. Therefore, the
437 decreases in isoprene, monoterpenes and sesquiterpenes mixing ratios in the WD-cut of 180-
438 240° were attributed to the reduced biogenic emissions of fewer Norway spruce and the dilution
439 effect caused by higher wind speeds. The dilution effect was supported by the lowest CO mixing
440 ratios and BC mass concentrations observed in the WD-cut of 180-240°.

441 Based on the above WD analyses, we further investigated the diurnal variations of
442 meteorological parameters as well as gas species in two major groups influenced by
443 anthropogenic (WD-BPP and WD-village) and biogenic (WD-forest and WD-cut) emissions
444 respectively (**Fig. 6**). In the anthropogenic-group, the diurnal variations of CH₄ mixing ratios
445 showed higher values during nighttime, which were related to the BPP emissions, low wind
446 speed and PBL height. However, a less pronounced diurnal variation of CH₄ mixing ratios was
447 observed under the influence of biogenic-group. In the anthropogenic-group, the diurnal
448 behavior of monoterpenes showed higher mixing ratios during nighttime but with large
449 fluctuations over the whole day. These fluctuations with monoterpene spikes were related to
450 the BPP emissions depending on the wind directions. As expected, isoprene showed higher
451 mixing ratios during daytime in the biogenic-group, which is similar to the diurnal behavior of
452 isoprene emission rate in previous observations in Norway spruce-dominated forests
453 (Bourtsoukidis et al., 2014; Juráň et al., 2017). However, in the biogenic-group, the diurnal
454 variations of monoterpenes and sesquiterpenes showed very low mixing ratios during daytime
455 due to the expanding PBL and strong photochemical consumption. The concentrations of
456 monoterpenes and sesquiterpenes peaked at ~18:00 when the concentrations of atmospheric
457 oxidants (OH radicals and O₃) and PBL heights decreased. Monoterpenes and sesquiterpenes
458 showed low mixing ratios with <1 ppb and <0.01 ppb, respectively after 18:00 during nighttime
459 in the biogenic-group. This is different with previous studies in the boreal forests where
460 constantly higher mixing ratios of monoterpenes and sesquiterpenes but lower O₃ values (<20
461 ppb) were observed during nighttime compared to daytime (Hakola et al., 2012; Li et al., 2020).
462 However, in our study, higher O₃ mixing ratios (~30 ppb) were observed during nighttime in
463 the biogenic-group, which may have reduced the concentrations of monoterpenes and
464 sesquiterpenes by nighttime oxidation. Note that the mixing ratios of monoterpenes and
465 sesquiterpenes were low during daytime, but they increased slightly from 8:00-12:00 when the
466 temperature and radiation increased. **Figure 7** shows the time series of isoprene, monoterpenes,
467 sesquiterpenes and O₃ along with wind direction, ambient temperature and radiation during low-
468 T and high-T episodes. During daytime of the high-T episode, we observed that the mixing
469 ratios of isoprene, monoterpenes, sesquiterpenes all increased as the temperature increased
470 when the sampling site was constantly influenced by the WD of ~100° from the intact forest.
471 Meanwhile, higher radiation and constantly high mixing ratios of O₃ (40-60 ppb) were observed
472 during daytime of the high-T episode. The photochemical O₃ production is supported by also
473 by higher BVOC mixing ratios. However, the increasing biogenic emissions due to higher
474 temperatures and solar radiation obviously exceeded the photochemical consumptions.

475 Similarly, higher mixing ratios of O₃ were observed during daytime of the low-T episode when
476 the sampling site was also constantly influenced by the wind direction of ~100° (e.g., 11th of
477 June). However, the mixing ratios of isoprene, monoterpenes, sesquiterpenes showed no
478 increase. In **Fig. 7a**, we also found that very high mixing ratios of monoterpenes and
479 sesquiterpenes during the low-T episode (e.g., 20:00-24:00, 10th of June) were associated with
480 the changes of wind directions, which was in line with the WD analyses as discussed above.
481 Besides, soil moisture showed no significant difference between the low-T and high-T episode
482 (**Fig. 2**). We cannot demonstrate the impact of soil moisture on the variations of BVOC mixing
483 ratios due to the observation period was short in this study.

484 **3.3 Source apportionment of VOCs**

485 In addition to meteorological impacts, the variations of VOC concentrations are influenced
486 by different emission sources and chemical processes. We performed a PMF analysis of Vocus-
487 PTR-ToF-MS-measured VOC data to identify and determine the impacts of different sources
488 and oxidation processes. According to the factor profiles and temporal variations, we present a
489 six-factor solution including one terpene-dominated factor, one factor related to BVOC
490 oxidation during nighttime, one factor related to aromatic VOC oxidation and three factors
491 related to daytime BVOC oxidation. **Figure 8** shows the factor profiles, time series and diurnal
492 variations of six factors as well as their relative contribution to total VOCs (TVOCs) during the
493 entire measurement campaign.

494 The first factor profile was dominated by the monoterpene parent ion (C₁₀H₁₇⁺) and its
495 fragment ion (C₆H₉⁺) (Tani et al., 2003; Kari et al., 2018). Furthermore, this factor was
496 characterized with higher fraction of monoterpenoids such as C₁₀H₁₇O⁺ (camphor or
497 monoterpene oxide) and C₁₀H₁₉O⁺ (linalool or monoterpene water cluster) in high mass range
498 (*m/z*140-230) (Li et al., 2020). These monoterpenoids can be emitted by leaves and flowers
499 directly (Joó et al., 2010). Therefore, we define this factor as a terpene-dominated factor. As
500 discussed before, the variations of monoterpene concentrations were influenced by the BPP
501 emissions and biogenic emissions depending on the wind directions. In this study, PMF analysis
502 could not separate the relative contribution of biogenic emissions and BPP emissions to
503 monoterpenes directly. This is probably due to the source profile of BPP emissions dominated
504 by the monoterpenes that is similar to that of biogenic emissions. Based on the WD analyses,
505 this factor was expected to be mainly associated with the biogenic emissions when the winds
506 were coming from the forest. In contrast, when the winds were coming from the BPP, this factor
507 was significantly contributed by the BPP emissions.

508 The second factor profile was characterized with high fractions of $C_{10}H_{17}O^+$ (monoterpene
509 oxide), $C_{10}H_{17}O_2^+$ and $C_{10}H_{15}O^+$ (pinonaldehyde and its fragment ion) in high mass range.
510 These compounds were weakly-oxidized products of monoterpenes with oxygen atom number
511 < 3 as found by previous studies (Li et al., 2021a; Li et al., 2020; Vermeuel et al., 2023). In
512 addition, this factor was dominated by $C_3H_7O^+$ (acetone), which could be contributed by the
513 primary emissions and the oxidation of VOCs from both biogenic and anthropogenic sources
514 (Jacob et al., 2002). The diurnal pattern of second factor showed higher concentrations at
515 nighttime. Therefore, we define this factor representing the secondary oxidation processes of
516 BVOCs especially monoterpenes during nighttime (night-SecVOC). Li et al., (2021a)
517 performed a binPMF analysis on Vocus-PTR-ToF-MS-measured VOC data at two European
518 forest sites. They also resolved a factor representing weakly-oxidized products of monoterpenes
519 with higher concentrations at night (Li et al., 2021a).

520 The third factor profile was characterized with higher fractions of $C_6H_7O^+$ (phenol),
521 $C_6H_7O_2^+$ (catechol), and $C_7H_7O_2^+$ (benzoic acid) compared to other factors. Furthermore, this
522 factor was dominated by $C_7H_9O_3^+$ (e.g., oxo-heptedienoic acid) and $C_8H_9O_3^+$ (e.g., vanillin) in
523 high mass range. These OVOC species could originate from the oxidation of aromatic
524 hydrocarbons (Hamilton et al., 2005; Zaytsev et al., 2019; Li et al., 2021b; Wu et al., 2014;
525 Lannuque et al., 2023). As expected, good correlations were found for aromatic OVOC with
526 catechol ($r = 0.87$ for $C_6H_7O_2^+$) and benzoic acid ($r = 0.84$ for $C_7H_7O_2^+$). In addition, this factor
527 also correlated well ($r = 0.77-0.87$, **Fig. S10**) with $C_5H_5O_3^+$ (e.g., methylfurandione), $C_5H_5O_2^+$
528 (e.g., butenedial), $C_4H_5O_2^+$ (e.g., furfural), and $C_3H_5O_2^+$ (e.g., methylglyoxal). These
529 compounds are likely ring-opening products of toluene oxidation as reported in previous studies
530 (Zaytsev et al., 2019; Wu et al., 2014; Lannuque et al., 2023). Therefore, we identified this
531 factor as a factor of aromatic OVOC representing the OVOCs formed from the oxidation of
532 aromatic hydrocarbons. The diurnal variation of aromatic OVOC factor showed slightly higher
533 concentrations during daytime, which can be related to an enhanced photochemical oxidation
534 of aromatic hydrocarbons.

535 In this study, we also resolved three factors related to the oxidation of BVOCs during
536 daytime denoted as day-SecVOC1, day-SecVOC2 and day-SecVOC3. The factor profile of
537 day-SecVOC1 was characterized with high fractions of acetic acid ($C_2H_5O_2^+$) as well as
538 isoprene and its oxidation products (e.g., $C_5H_9^+$, $C_4H_7O_{1-4}^+$ and $C_5H_9O_{2-4}^+$). This factor was also
539 dominated by stronger oxidized products of monoterpenes with oxygen atom numbers >3 (e.g.,
540 $C_{10}H_{17}O_{4-5}^+$) compared to other factors in the higher mass range. The diurnal variations of day-

541 SecVOC1 factor showed high concentrations during daytime. Therefore, the day-SecVOC1
542 factor can be mainly attributed to the photochemical oxidation of isoprene and monoterpenes
543 during daytime. Li et al., (2021a) resolved one factor representing isoprene and its oxidation
544 products and another factor representing stronger oxidized products of monoterpenes from the
545 binPMF analysis for a low-mass (m_z 50-200) and a high-mass range (m_z 201-320), respectively,
546 for two European forest sites. They found that these two factors had a similar diurnal pattern
547 with high daytime concentrations. In our study, we performed the PMF analysis for the full
548 mass range (m/z 40-230) of the major VOC ions and resolved the day-SecVOC1 factor
549 containing high fractions of oxidized products of isoprene and monoterpenes. This suggests that
550 isoprene oxidation products and higher oxidized products of monoterpenes were mainly related
551 to the daytime oxidation processes. The factor profiles of both day-SecVOC2 and day-
552 SecVOC3 were characterized with high fractions of acetone ($C_3H_7O^+$) and acetic acid
553 ($C_2H_5O_2^+$). Acetone and acetic acid could be contributed by biogenic and anthropogenic
554 secondary sources (Khare et al., 1999; Jacob et al., 2002). The factor profile of day-SecVOC2
555 also had high fractions of $C_2H_7O_3^+$ (acetic acid water cluster), $C_3H_7O_2^+$ (propionic acid),
556 $C_4H_9O_2^+$ (butyric acid) and $C_3H_9O_2^+$ (e.g., propylene glycol). These gaseous organic acids could
557 be formed from the oxidation of BVOCs like monoterpenes (Friedman and Farmer, 2018). In
558 addition, the factor profile of day-SecVOC3 showed higher fractions of $C_4H_7O_4^+$ (e.g., succinic
559 acid) compared to other factors. The time series of day-SecVOC3 showed the highest
560 correlations with $C_2H_7O_3^+$ (acetic acid water cluster, $r = 0.79$), $C_2H_5O_2^+$ (acetic acid, $r = 0.63$)
561 and $C_3H_9O_3^+$ (propionic acid water cluster) compared to other factors. The time series of day-
562 SecVOC3 factor also showed strong correlations with $C_4H_6O^+$ ($r = 0.90$, **Fig. S10**) and $C_2H_5O_3^+$
563 ($r = 0.89$), which can be assigned as the isoprene oxidation product as deprotonated $C_4H_7O^+$
564 (MVK+MACR) and glycolic acid, respectively. In addition, O_3 was only weakly correlated
565 with day-SecVOC2 ($r = 0.27$), but much better correlated with day-SecVOC3 ($r = 0.57$).
566 Moreover, a better correlation was found between O_3 and the sum of these two factors ($r =$
567 0.70). The diurnal variations of both factors showed higher concentrations during daytime.
568 Based on these results, we identified day-SecVOC2 and day-SecVOC3 as representing low-
569 molecular weight oxygenated organic compounds produced from the daytime photooxidation
570 of BVOCs.

571 As shown in **Fig. 8**, the mixing ratios of TVOCs measured by the Vocus-PTR-ToF-MS for
572 the PMF analysis was 9.0 ± 4.4 ppb during the entire campaign. The mixing ratios of TVOCs
573 was dominated by the daytime BVOC oxidation with day-SecVOC1 ($8\% \pm 5\%$), day-SecVOC2
574 ($27\% \pm 20\%$), day-SecVOC3 ($18\% \pm 21\%$). This indicates substantial contributions of

575 oxygenated species to TVOCs during the entire campaign. Based on the WD analysis, we
576 further compared the relative contributions of VOC factors to TVOCs for the groups influenced
577 by the biogenic and anthropogenic emissions, respectively. The average mixing ratios of
578 TVOCs in the biogenic-group (9.7 ± 4.7 ppb) were slightly higher than that in the
579 anthropogenic-group (7.1 ± 3.6 ppb). The contribution of day-SecVOC2 to TVOCs was
580 comparable with $25\% \pm 21\%$ and $32\% \pm 18\%$ for the biogenic- and anthropogenic-group,
581 respectively. However, the contribution of day-SecVOC3 to TVOCs in the biogenic-group
582 ($26\% \pm 25\%$) was higher than that in the anthropogenic-group ($13\% \pm 15\%$). We observed
583 significantly elevated mixing ratios of isoprene (**Fig. 3c**) and day-SecVOC3 during the high-T
584 episode (**Fig. 8**). As mentioned before, the sampling site was mainly influenced by the winds
585 coming from the intact forest during high-T episode along with higher mixing ratios of O_3 .
586 Therefore, higher contribution of day-SecVOC3 in the biogenic-group was attributed to the
587 strong oxidation of BVOCs especially of isoprene. The contribution of terpene-dominated
588 factor to TVOCs was higher in the anthropogenic-group ($18\% \pm 16\%$) compared to that in the
589 biogenic-group ($11\% \pm 15\%$). This is consistent with the WD analyses that higher monoterpene
590 mixing ratios were related to the BPP emissions. In addition, the contributions of night-SecVOC
591 and day-SecVOC1 factors to TVOCs concentrations were slightly higher in the anthropogenic-
592 group, which were related to high abundances of monoterpenes. Furthermore, gas-to-particle
593 partitioning processes could also influence the variations of BVOC oxidation products and thus
594 night-SecVOC and day-SecVOC1 factors.

595 **3.4 Variations of BVOC oxidation products in gas- and particle phases**

596 **Figure 9** shows the diurnal variations of concentrations of organic molecules ($C_5H_9O_{1-4}^+$,
597 $C_4H_7O_{1-4}^+$, $C_{10}H_{17}O_{1-5}^+$ and $C_{10}H_{15}O_{1-5}^+$) in the gas phase measured by the Vocus-PTR-ToF-
598 MS and particle phase compounds measured by the CHARON-PTR-ToF-MS during 22nd-30th
599 of June. These organic molecules are important components of night-SecVOC and day-
600 SecVOC1 factors resolved by the PMF analysis, and they are identified as the oxidation
601 products from isoprene and monoterpenes based on previous field observations and simulation
602 chamber experiments (Gkatzelis et al., 2018; Li et al., 2020). For example, gaseous $C_4H_7O^+$ can
603 be the sum of methyl vinyl ketone (MVK) and methacrolein (MACR), which are major products
604 of the isoprene oxidation (Wennberg et al., 2018). $C_{10}H_{17}O_3^+$ can be attributed to *cis*-pinonic
605 acid formed from the oxidation of monoterpenes (e.g., α -pinene). Again, the fragmentation of
606 high-molecular weight oxidized organic compounds measured by the PTR-ToF-MS
607 instruments could produce the fragment ions via the loss of neutral water, carbonyl, or carboxyl

608 groups (-H₂O, -CO and -CO₂). The diurnal variations of all isoprene oxidation products
609 (C₅H₉O₁₋₄⁺ and C₄H₇O₁₋₄⁺) in both gas and particle phases showed higher concentrations from
610 morning (6:00-8:00) to afternoon (12:00-16:00) as well as isoprene itself. These results indicate
611 that higher temperatures and intensive sunlight not only favor the isoprene emissions but also
612 enhance photochemical oxidation of isoprene. Besides, we found that the concentrations of
613 particulate C₄H₇O₁₋₂⁺ showed increased values from early nighttime (18:00-20:00) to midnight
614 (0:00-2:00 of the next day). As mentioned before, the fragmentation of *cis*-pinonic acid in the
615 CHARON-PTR-ToF-MS can produce the fragment ions C₄H₇O⁺, C₆H₁₁O₂⁺ and C₁₀H₁₅O₂⁺
616 (Gkatzelis et al., 2018; Peng et al., 2023; Muller et al., 2017; Leglise et al., 2019). Furthermore,
617 we observed a similar diurnal pattern of C₄H₇O⁺ and C₁₀H₁₅O₂⁺ in the particle phase, suggesting
618 that the nighttime increase of particulate C₄H₇O⁺ was likely contributed by the fragmentation
619 of *cis*-pinonic acid. Due to instrumental limitation, it is difficult to assign each ion detected by
620 the PTR-ToF-MS to either parent ion or fragment ion of one organic compound in the ambient
621 particles.

622 The diurnal variations of weakly-oxidized products of monoterpenes like C₁₀H₁₇O₁₋₂⁺ and
623 C₁₀H₁₅O₁₋₂⁺ in both gas and particle phases showed elevated concentrations during nighttime.
624 In contrast, the more-oxidized products of monoterpenes (C₁₀H₁₇O₄₋₅⁺ and C₁₀H₁₅O₄₋₅⁺) showed
625 higher concentrations in gas and particle phases during daytime. The higher atmospheric
626 oxidation capacity during daytime compared to nighttime leads to the formation of more-
627 oxidized products. In addition, C₁₀H₁₇O₃⁺ (*cis*-pinonic acid) and its fragment ion (C₁₀H₁₅O₂⁺)
628 in the gas phase showed less pronounced diurnal patterns. The particulate C₁₀H₁₇O₃⁺ also
629 showed a less pronounced diurnal behavior, while the particulate C₁₀H₁₅O₂⁺ showed increased
630 concentrations during nighttime. This is in agreement with previous findings that most of the
631 particulate compounds detected by the CHARON-PTR-ToF-MS were not detected as the parent
632 ion but as the fragment ion with one H₂O molecule lost (Gkatzelis et al., 2018). In this study,
633 C₁₄H₂₃O₂⁺, C₁₅H₂₃O⁺, C₁₅H₂₅O₂⁺ were measured by the PTR instruments, which can be
634 considered as the sesquiterpene oxidation products based on previous field and simulation
635 chamber studies. Here C₁₄H₂₃O₂⁺ was detected only in the gas phase by the Vocus-PTR-ToF-
636 MS, while C₁₅H₂₃O₂⁺ and C₁₅H₂₅O₂⁺ were detected only in the particle phase by the CHARON-
637 PTR-ToF-MS. The concentrations of sesquiterpene oxidation products in both gas (<0.5 ppt)
638 and particle phases (<5 ng m⁻³) were relatively low probably due to correspondingly low
639 concentrations of sesquiterpenes in this study. The diurnal pattern of gaseous C₁₄H₂₃O₂⁺ showed
640 two peaks in the morning and early evening (**Fig. S11**), which was similar to those of weakly-
641 oxidized products of sesquiterpenes (e.g., C₁₄H₂₂O₁₋₃ and C₁₅H₂₄O₁₋₃) observed at the Landes

642 forest in France (Li et al., 2020). The diurnal variations of particulate $C_{15}H_{23}O_2^+$ and $C_{15}H_{25}O_2^+$
643 showed slightly higher values during nighttime.

644 Furthermore, we calculated the variations of $OA/\Delta CO$, which are the total OA
645 concentrations measured by the CHARON-PTR-ToF-MS normalized over ΔCO (subtracted by
646 the background CO concentration) during 22nd-30th of June (**Fig. 10**). CO is relatively long-
647 lived, normalizing the observed OA mass concentrations to the background-corrected CO helps
648 to minimize the impacts of boundary layer dynamics (De Gouw and Jimenez, 2009). An
649 increase of $OA/\Delta CO$ was observed during nighttime of the high-T episode, which could be
650 related to the gas-to-particle partitioning of BVOC oxidation products. Based on the two PTR
651 measurements, we calculated the particulate fraction of representative monoterpene oxidation
652 products (i.e., $C_{10}H_{17}O_{1-3}^+$ and $C_{10}H_{15}O_{1-5}^+$) to estimate their gas gas-to-particle partitioning
653 processes. The two PTR instruments used in this study may have different sensitivities or
654 fragmentation for different oxygenated organic compounds. For example, the concentrations of
655 monoterpene oxidation products such as $C_9H_{15}O^+$, $C_{10}H_{15}O_{1-2}^+$ and $C_{10}H_{17}^+$ measured by the
656 Vocus-PTR-ToF-MS were ~2-3 times higher than those measured by the CHARON-PTR-ToF-
657 MS (**Fig. S13b**). Although we cannot precisely calculate the F_p values for each OA molecule
658 due to instrumental limitations, the variations of calculated F_p values can still be used as an
659 indicator for estimating the gas-to-particle portioning processes. As shown in **Fig. 10**, weakly-
660 oxidized molecules of monoterpenes ($C_{10}H_{17}O_{1-2}^+$ and $C_{10}H_{15}O_{1-3}^+$) had lower F_p values
661 compared to more-oxidized molecules of monoterpenes ($C_{10}H_{17}O_3^+$ and $C_{10}H_{15}O_{4-5}^+$). This is
662 expected because more-oxidized products of monoterpenes generally have lower volatility
663 compared to weakly-oxidized ones. Interestingly, the F_p values of weakly-oxidized molecules
664 of monoterpenes showed similar temporal trends as the relative humidity. Especially for the
665 high-T episode, the F_p values of weakly-oxidized molecules of monoterpenes ($C_{10}H_{15}O_{1-3}^+$)
666 showed positive correlations ($r = 0.65-0.71$) with RH. This indicates that increasing RH can
667 enhance the particle fraction of weakly-oxidized molecules of monoterpenes and thus increase
668 SOA mass. As validated in Section 3.3, these weakly-oxidized molecules of monoterpenes are
669 formed by oxidation of monoterpenes emitted from trees during the high-T episode rather than
670 from BPP emissions. It is reasonable to assume that these monoterpenes are mainly α -pinene
671 and β -pinene because our sampling site was in a forest dominated by Norway spruce known to
672 emit mainly pinenes (Christensen et al., 2000; Hakola et al., 2017). Previously, Tillmann et al.,
673 (2010) found that the SOA yields from the ozonolysis of α -pinene were higher at humid
674 conditions than at dry conditions. More recently, Surdu et al., (2023) studied the effect of RH
675 on the partitioning of oxidized organic molecules formed from α -pinene oxidation at the CERN

676 CLOUD chamber. They observed that the particle-phase concentrations of semi-volatile
677 organic molecules ($C_{10}H_{16}O_{2-3}$) from α -pinene oxidation significantly increases by factors of 2-
678 4 with increasing RH, thus leading to a substantial increase of SOA mass (Surdu et al., 2023).
679 Similarly, Luo et al., (2024) reported that increasing RH from 3% to 84% increase the
680 abundance of less oxidized products (e.g., $C_{10}H_{16}O_{2-6}$) from α -pinene ozonolysis. In our study,
681 during the high-T episode, we observed the F_p values for $C_{10}H_{15}O^+$, $C_{10}H_{15}O_2^+$ and $C_{10}H_{15}O_3^+$
682 increased by ~2%, ~6% and ~20% respectively when RH was increased from 30-40% to 60-
683 80%. Besides, the ambient temperature was anticorrelated with RH in this study. Thus, lower
684 temperatures may further additionally favor the gas-to-particle partitioning of semi-volatile
685 organic molecules from monoterpene oxidation.

686 **4 Conclusions**

687 In this study, we investigated the characteristics of VOCs and OA particles simultaneously
688 measured by a CHARON-PTR-ToF-MS and a Vocus-PTR-ToF-MS at a Norway spruce-
689 dominated forest stressed by bark beetles and droughts close to a BPP in western Germany
690 during June 2020. The average mass concentration of OA particles detected by the CHARON-
691 PTR-ToF-MS was $0.8 \pm 0.5 \mu\text{g m}^{-3}$. The chemical composition of OA ions ranged between C_2
692 and C_{10} with oxygen atom numbers of 0-5, which were mainly attributed to the semi-volatile
693 organic compounds formed from monoterpene oxidation. The average mixing ratios of isoprene
694 and monoterpenes were higher than the values previously measured in both German temperate
695 forests and boreal forests during summertime (Mermert et al., 2021; Li et al., 2021a; Hellén et
696 al., 2018; Bourtsoukidis et al., 2014) which may be due to stressed trees with long lasting
697 droughts and bark beetle infestation and differences in the meteorological conditions. Based on
698 the WD analyses, BVOC data were categorized into two groups to distinguish the impacts of
699 biogenic emissions from an intact forest and a clear cut (biogenic-group) and anthropogenic
700 emissions from a BPP and a village (anthropogenic-group). The mixing ratios of CH_4 and
701 monoterpenes showed significantly higher values in the anthropogenic-group. This was
702 expected for CH_4 , and it is also known that BPP can release high concentrations of
703 monoterpenes during biowaste storage and fermentation processes (Salazar Gómez et al., 2016;
704 Papurello et al., 2012). In the biogenic-group, the variations in mixing ratios of isoprene,
705 monoterpenes and sesquiterpenes were driven by the interplay between meteorological
706 conditions, biogenic emissions and subsequent chemical oxidation processes. Based on the
707 PMF analysis of VOCs measured by the Vocus-PTR-ToF-MS, six factors were resolved,
708 representing the major sources and/or products of chemical transformation processes. During

709 the entire measurement period, TVOCs were largely composed of oxygenated organic
710 compounds formed from the photochemical oxidation of BVOCs during daytime. However,
711 monoterpenes and their weakly-oxidized products (e.g., $C_{10}H_{15}O_{1-3}^+$ and $C_{10}H_{17}O_{1-2}^+$)
712 dominated the TVOCs during nighttime. These weakly-oxidized monoterpene products in the
713 particle phase also showed higher concentrations during nighttime. In contrast, more-oxidized
714 monoterpene products (e.g., $C_{10}H_{17}O_{4-5}^+$ and $C_{10}H_{15}O_{4-5}^+$) in both gas and particle phases were
715 more abundant during daytime. By combining the gas and particle data measured by the
716 CHARON-PTR-ToF-MS and the Vocus-PTR-ToF-MS, we found that increasing RH and
717 decreasing temperature led to an increase in the particulate fraction of weakly-oxidized
718 monoterpene products, consistent with the findings from recent simulation chamber studies
719 (Surdu et al., 2023; Luo et al., 2024). Overall, this study demonstrates that the variations of
720 BVOCs are influenced not only by meteorology and biogenic emissions but also by local
721 anthropogenic emissions (e.g., from a BPP), and subsequent chemical transformation processes
722 in a typical stressed European coniferous forest. The impact of soil moisture, tree species
723 composition and tree health conditions on the variations of BVOC concentrations could not be
724 fully addressed due to the relative short observation period. Future long-term field
725 measurements including seasonality and detailed tree characterization are necessary to assess
726 the impacts of droughts and bark beetle outbreaks on BVOC emissions and subsequent
727 formation of SOA.

728

729 **Data availability**

730 Data shown in this paper are available via the KIT open data portal
731 (<https://doi.org/10.35097/qbwwf0p62zksrkwj>, Song et al., 2024).

732

733 **Author contributions**

734 JS, HS and RT conducted the field measurements. JS and GG carried out the data analysis of
735 CHARON-PTR-ToF-MS and Vocus-PTR-ToF-MS respectively. NB and TL gave general
736 comments for this paper. JS drafted the manuscript with contributions from all co-authors.

737 **Competing interest**

738 At least one of the (co-)authors is a member of the editorial board of Atmospheric Chemistry
739 and Physics.

740 **Acknowledgement**

741 This work was supported by the Modular Observation Solutions for Earth Systems (MOSES)
742 project, a novel observing system of the Helmholtz Association. Financial support by China
743 Scholarship Council (CSC) for JS is gratefully acknowledged. We gratefully acknowledged the
744 TERENO (Terrestrial Environmental Observatories) funded by the Helmholtz-Gemeinschaft.
745 The authors acknowledged Heye Bogena for providing daily soil moisture data as well as
746 Christian Wesolek, Sergej Wedel, and Doreen Niether for their technical support in field
747 measurement deployment.

748

749 **References**

- 750 Atkinson, R.: Atmospheric chemistry of VOCs and NO_x, *Atmos. Environ.*, 34, 2063-2101,
751 [https://doi.org/10.1016/S1352-2310\(99\)00460-4](https://doi.org/10.1016/S1352-2310(99)00460-4), 2000.
- 752 Bakkaloglu, S., Lowry, D., Fisher, R. E., France, J. L., Brunner, D., Chen, H., and Nisbet, E. G.:
753 Quantification of methane emissions from UK biogas plants, *Waste Manag.*, 124, 82-93,
754 <https://doi.org/10.1016/j.wasman.2021.01.011>, 2021.
- 755 Bogena, H. R., Huisman, J. A., Güntner, A., Hübner, C., Kusche, J., Jonard, F., Vey, S., and Vereecken,
756 H.: Emerging methods for noninvasive sensing of soil moisture dynamics from field to catchment
757 scale: a review, *WIREs Water*, 2, 635-647, <https://doi.org/10.1002/wat2.1097>, 2015.
- 758 Bonn, B., Magh, R. K., Rombach, J., and Kreuzwieser, J.: Biogenic isoprenoid emissions under drought
759 stress: different responses for isoprene and terpenes, *Biogeosciences*, 16, 4627-4645, 10.5194/bg-
760 16-4627-2019, 2019.
- 761 Bourtsoukidis, E., Williams, J., Kesselmeier, J., Jacobi, S., and Bonn, B.: From emissions to ambient
762 mixing ratios: online seasonal field measurements of volatile organic compounds over a Norway
763 spruce-dominated forest in central Germany, *Atmos. Chem. Phys.*, 14, 6495-6510, 10.5194/acp-14-
764 6495-2014, 2014.
- 765 Bourtsoukidis, E., Pozzer, A., Williams, J., Makowski, D., Peñuelas, J., Matthaios, V. N., Lazoglou, G.,
766 Yañez-Serrano, A. M., Lelieveld, J., Ciais, P., Vrekoussis, M., Daskalakis, N., and Sciare, J.: High
767 temperature sensitivity of monoterpene emissions from global vegetation, *Commun. Earth Environ.*,
768 5, 23, 10.1038/s43247-023-01175-9, 2024.
- 769 Brémond, U., Bertrandias, A., Steyer, J.-P., Bernet, N., and Carrere, H.: A vision of European biogas
770 sector development towards 2030: Trends and challenges, *J. Clean. Prod.*, 287, 125065,
771 <https://doi.org/10.1016/j.jclepro.2020.125065>, 2021.
- 772 Byron, J., Kreuzwieser, J., Purser, G., van Haren, J., Ladd, S. N., Meredith, L. K., Werner, C., and
773 Williams, J.: Chiral monoterpenes reveal forest emission mechanisms and drought responses,
774 *Nature*, 609, 307-312, 10.1038/s41586-022-05020-5, 2022.
- 775 Christensen, C. S., Hummelshøj, P., Jensen, N. O., Larsen, B., Lohse, C., Pilegaard, K., and Skov, H.:
776 Determination of the terpene flux from orange species and Norway spruce by relaxed eddy
777 accumulation, *Atmos. Environ.*, 34, 3057-3067, [https://doi.org/10.1016/S1352-2310\(99\)00502-6](https://doi.org/10.1016/S1352-2310(99)00502-6),
778 2000.
- 779 De Gouw, J. and Jimenez, J. L.: Organic Aerosols in the Earth's Atmosphere, *Environ. Sci. Technol.*,
780 43, 7614-7618, 10.1021/es9006004, 2009.
- 781 Desservettaz, M., Pikridas, M., Stavroulas, I., Bougiatioti, A., Liakakou, E., Hatzianastassiou, N., Sciare,
782 J., Mihalopoulos, N., and Bourtsoukidis, E.: Emission of volatile organic compounds from
783 residential biomass burning and their rapid chemical transformations, *Sci. Total Environ.*, 903,
784 166592, <https://doi.org/10.1016/j.scitotenv.2023.166592>, 2023.
- 785 Eichler, P., Müller, M., D'Anna, B., and Wisthaler, A.: A novel inlet system for online chemical analysis
786 of semi-volatile submicron particulate matter, *Atmos. Meas. Tech.*, 8, 1353-1360, 10.5194/amt-8-
787 1353-2015, 2015.
- 788 Faiola, C. and Taipale, D.: Impact of insect herbivory on plant stress volatile emissions from trees: A
789 synthesis of quantitative measurements and recommendations for future research, *Atmos. Environ.*:
790 X., 5, 100060, <https://doi.org/10.1016/j.aeaoa.2019.100060>, 2020.
- 791 Friedman, B. and Farmer, D. K.: SOA and gas phase organic acid yields from the sequential
792 photooxidation of seven monoterpenes, *Atmos. Environ.*, 187, 335-345,
793 <https://doi.org/10.1016/j.atmosenv.2018.06.003>, 2018.
- 794 Ghimire, R. P., Kivimäenpää, M., Blomqvist, M., Holopainen, T., Lyytikäinen-Saarenmaa, P., and
795 Holopainen, J. K.: Effect of bark beetle (*Ips typographus* L.) attack on bark VOC emissions of
796 Norway spruce (*Picea abies* Karst.) trees, *Atmos. Environ.*, 126, 145-152,
797 <https://doi.org/10.1016/j.atmosenv.2015.11.049>, 2016.
- 798 Gkatzelis, G. I., Coggon, M. M., McDonald, B. C., Peischl, J., Gilman, J. B., Aikin, K. C., Robinson,
799 M. A., Canonaco, F., Prevot, A. S. H., Trainer, M., and Warneke, C.: Observations Confirm that
800 Volatile Chemical Products Are a Major Source of Petrochemical Emissions in U.S. Cities, *Environ.*
801 *Sci. Technol.*, 55, 4332-4343, 10.1021/acs.est.0c05471, 2021.
- 802 Gkatzelis, G. I., Tillmann, R., Hohaus, T., Müller, M., Eichler, P., Xu, K. M., Schlag, P., Schmitt, S. H.,
803 Wegener, R., Kaminski, M., Holzinger, R., Wisthaler, A., and Kiendler-Scharr, A.: Comparison of

804 three aerosol chemical characterization techniques utilizing PTR-ToF-MS: a study on freshly
805 formed and aged biogenic SOA, *Atmos. Meas. Tech.*, 11, 1481-1500, 10.5194/amt-11-1481-2018,
806 2018.

807 Guenther, A. B., Jiang, X., Heald, C. L., Sakulyanontvittaya, T., Duhl, T., Emmons, L. K., and Wang,
808 X.: The Model of Emissions of Gases and Aerosols from Nature version 2.1 (MEGAN2.1): an
809 extended and updated framework for modeling biogenic emissions, *Geosci. Model Dev.*, 5, 1471-
810 1492, 10.5194/gmd-5-1471-2012, 2012.

811 Hakola, H., Hellén, H., Hemmilä, M., Rinne, J., and Kulmala, M.: In situ measurements of volatile
812 organic compounds in a boreal forest, *Atmos. Chem. Phys.*, 12, 11665-11678, 10.5194/acp-12-
813 11665-2012, 2012.

814 Hakola, H., Tarvainen, V., Praplan, A. P., Jaars, K., Hemmilä, M., Kulmala, M., Bäck, J., and Hellén,
815 H.: Terpenoid and carbonyl emissions from Norway spruce in Finland during the growing season,
816 *Atmos. Chem. Phys.*, 17, 3357-3370, 10.5194/acp-17-3357-2017, 2017.

817 Hallquist, M., Wenger, J. C., Baltensperger, U., Rudich, Y., Simpson, D., Claeys, M., Dommen, J.,
818 Donahue, N. M., George, C., Goldstein, A. H., Hamilton, J. F., Herrmann, H., Hoffmann, T., Iinuma,
819 Y., Jang, M., Jenkin, M. E., Jimenez, J. L., Kiendler-Scharr, A., Maenhaut, W., McFiggans, G.,
820 Mentel, T. F., Monod, A., Prévôt, A. S. H., Seinfeld, J. H., Surratt, J. D., Szmigielski, R., and Wildt,
821 J.: The formation, properties and impact of secondary organic aerosol: current and emerging issues,
822 *Atmos. Chem. Phys.*, 9, 5155-5236, 10.5194/acp-9-5155-2009, 2009.

823 Hamilton, J. F., Webb, P. J., Lewis, A. C., and Reviejo, M. M.: Quantifying small molecules in
824 secondary organic aerosol formed during the photo-oxidation of toluene with hydroxyl radicals,
825 *Atmos. Environ.*, 39, 7263-7275, <https://doi.org/10.1016/j.atmosenv.2005.09.006>, 2005.

826 Hellén, H., Praplan, A. P., Tykkä, T., Ylivinkka, I., Vakkari, V., Bäck, J., Petäjä, T., Kulmala, M., and
827 Hakola, H.: Long-term measurements of volatile organic compounds highlight the importance of
828 sesquiterpenes for the atmospheric chemistry of a boreal forest, *Atmos. Chem. Phys.*, 18, 13839-
829 13863, 10.5194/acp-18-13839-2018, 2018.

830 Hersbach, H., Bell, B., Berrisford, P., Hirahara, S., Horányi, A., Muñoz-Sabater, J., Nicolas, J., Peubey,
831 C., Radu, R., Schepers, D., Simmons, A., Soci, C., Abdalla, S., Abellan, X., Balsamo, G., Bechtold,
832 P., Biavati, G., Bidlot, J., Bonavita, M., De Chiara, G., Dahlgren, P., Dee, D., Diamantakis, M.,
833 Dragani, R., Flemming, J., Forbes, R., Fuentes, M., Geer, A., Haimberger, L., Healy, S., Hogan, R.
834 J., Hólm, E., Janisková, M., Keeley, S., Laloyaux, P., Lopez, P., Lupu, C., Radnoti, G., de Rosnay,
835 P., Rozum, I., Vamborg, F., Villaume, S., and Thépaut, J.-N.: The ERA5 global reanalysis, *Q. J. R.
836 Meteorol. Soc.*, 146, 1999-2049, <https://doi.org/10.1002/qj.3803>, 2020.

837 Huang, W., Saathoff, H., Shen, X., Ramisetty, R., Leisner, T., and Mohr, C.: Chemical Characterization
838 of Highly Functionalized Organonitrates Contributing to Night-Time Organic Aerosol Mass
839 Loadings and Particle Growth, *Environ. Sci. Technol.*, 53, 1165-1174, 10.1021/acs.est.8b05826,
840 2019.

841 Huang, W., Li, H., Sarnela, N., Heikkinen, L., Tham, Y. J., Mikkilä, J., Thomas, S. J., Donahue, N. M.,
842 Kulmala, M., and Bianchi, F.: Measurement report: Molecular composition and volatility of gaseous
843 organic compounds in a boreal forest – from volatile organic compounds to highly oxygenated
844 organic molecules, *Atmos. Chem. Phys.*, 21, 8961-8977, 10.5194/acp-21-8961-2021, 2021.

845 Isaacman-VanWertz, G., Yee, L. D., Kreisberg, N. M., Wernis, R., Moss, J. A., Hering, S. V., de Sá, S.
846 S., Martin, S. T., Alexander, M. L., Palm, B. B., Hu, W., Campuzano-Jost, P., Day, D. A., Jimenez,
847 J. L., Riva, M., Surratt, J. D., Viegas, J., Manzi, A., Edgerton, E., Baumann, K., Souza, R., Artaxo,
848 P., and Goldstein, A. H.: Ambient Gas-Particle Partitioning of Tracers for Biogenic Oxidation,
849 *Environ. Sci. Technol.*, 50, 9952-9962, 10.1021/acs.est.6b01674, 2016.

850 Jaakkola, E., Gärtner, A., Jönsson, A. M., Ljung, K., Olsson, P. O., and Holst, T.: Spruce bark beetles
851 (*Ips typographus*) cause up to 700 times higher bark BVOC emission rates compared to healthy
852 Norway spruce (*Picea abies*), *Biogeosciences*, 20, 803-826, 10.5194/bg-20-803-2023, 2023.

853 Jacob, D. J., Field, B. D., Jin, E. M., Bey, I., Li, Q., Logan, J. A., Yantosca, R. M., and Singh, H. B.:
854 Atmospheric budget of acetone, *J. Geophys. Res. Atmos.*, 107, ACH 5-1-ACH 5-17,
855 <https://doi.org/10.1029/2001JD000694>, 2002.

856 Jain, V., Tripathi, N., Tripathi, S. N., Gupta, M., Sahu, L. K., Murari, V., Gaddamidi, S., Shukla, A. K.,
857 and Prevot, A. S. H.: Real-time measurements of non-methane volatile organic compounds in the
858 central Indo-Gangetic basin, Lucknow, India: source characterisation and their role in O₃ and

859 secondary organic aerosol formation, *Atmos. Chem. Phys.*, 23, 3383-3408, 10.5194/acp-23-3383-
860 2023, 2023.

861 Joó, É., Van Langenhove, H., Šimpraga, M., Steppe, K., Amelynck, C., Schoon, N., Müller, J. F., and
862 Dewulf, J.: Variation in biogenic volatile organic compound emission pattern of *Fagus sylvatica* L.
863 due to aphid infection, *Atmos. Environ.*, 44, 227-234,
864 <https://doi.org/10.1016/j.atmosenv.2009.10.007>, 2010.

865 Jordan, A., Haidacher, S., Hanel, G., Hartungen, E., Mark, L., Seehauser, H., Schotchkowsky, R., Sulzer,
866 P., and Mark, T. D.: A high resolution and high sensitivity proton-transfer-reaction time-of-flight
867 mass spectrometer (PTR-TOF-MS), *Int. J. Mass. Spectrom.*, 286, 122-128,
868 10.1016/j.ijms.2009.07.005, 2009.

869 Juráň, S., Pallozzi, E., Guidolotti, G., Fares, S., Šigut, L., Calfapietra, C., Alivernini, A., Savi, F.,
870 Večeřová, K., Krůmal, K., Večeřa, Z., and Urban, O.: Fluxes of biogenic volatile organic compounds
871 above temperate Norway spruce forest of the Czech Republic, *Agric. For. Meteorol.*, 232, 500-513,
872 <https://doi.org/10.1016/j.agrformet.2016.10.005>, 2017.

873 Kari, E., Miettinen, P., Yli-Pirilä, P., Virtanen, A., and Faiola, C. L.: PTR-ToF-MS product ion
874 distributions and humidity-dependence of biogenic volatile organic compounds, *Int. J. Mass.
875 Spectrom.*, 430, 87-97, <https://doi.org/10.1016/j.ijms.2018.05.003>, 2018.

876 Kari, E., Faiola, C. L., Isokääntä, S., Miettinen, P., Yli-Pirilä, P., Buchholz, A., Kivimäenpää, M.,
877 Mikkonen, S., Holopainen, J. K., and Virtanen, A.: Time-resolved characterization of biotic stress
878 emissions from Scots pines being fed upon by pine weevil by means of PTR-ToF-MS, *Boreal
879 Environ. Res.*, 24, 25-49, 2019.

880 Khare, P., Kumar, N., Kumari, K. M., and Srivastava, S. S.: Atmospheric formic and acetic acids: An
881 overview, *Rev. Geophys.*, 37, 227-248, <https://doi.org/10.1029/1998RG900005>, 1999.

882 Kleist, E., Mentel, T. F., Andres, S., Bohne, A., Folkers, A., Kiendler-Scharr, A., Rudich, Y., Springer,
883 M., Tillmann, R., and Wildt, J.: Irreversible impacts of heat on the emissions of monoterpenes,
884 sesquiterpenes, phenolic BVOC and green leaf volatiles from several tree species, *Biogeosciences*,
885 9, 5111-5123, 10.5194/bg-9-5111-2012, 2012.

886 Krechmer, J., Lopez-Hilfiker, F., Koss, A., Hutterli, M., Stoermer, C., Deming, B., Kimmel, J.,
887 Warneke, C., Holzinger, R., Jayne, J., Worsnop, D., Fuhrer, K., Gonin, M., and de Gouw, J.:
888 Evaluation of a New Reagent-Ion Source and Focusing Ion-Molecule Reactor for Use in Proton-
889 Transfer-Reaction Mass Spectrometry, *Anal. Chem.*, 90, 12011-12018,
890 10.1021/acs.analchem.8b02641, 2018.

891 Lannuque, V., D'Anna, B., Kostenidou, E., Couvidat, F., Martinez-Valiente, A., Eichler, P., Wisthaler,
892 A., Müller, M., Temime-Roussel, B., Valorso, R., and Sartelet, K.: Gas-particle partitioning of
893 toluene oxidation products: an experimental and modeling study, *Atmos. Chem. Phys.*, 23, 15537-
894 15560, 10.5194/acp-23-15537-2023, 2023.

895 Lee, B. H., Lopez-Hilfiker, F. D., D'Ambro, E. L., Zhou, P., Boy, M., Petäjä, T., Hao, L., Virtanen, A.,
896 and Thornton, J. A.: Semi-volatile and highly oxygenated gaseous and particulate organic
897 compounds observed above a boreal forest canopy, *Atmos. Chem. Phys.*, 18, 11547-11562,
898 10.5194/acp-18-11547-2018, 2018.

899 Leglise, J., Müller, M., Piel, F., Otto, T., and Wisthaler, A.: Bulk Organic Aerosol Analysis by Proton-
900 Transfer-Reaction Mass Spectrometry: An Improved Methodology for the Determination of Total
901 Organic Mass, O:C and H:C Elemental Ratios, and the Average Molecular Formula, *Anal. Chem.*,
902 91, 12619-12624, 10.1021/acs.analchem.9b02949, 2019.

903 Li, H., Riva, M., Rantala, P., Heikkinen, L., Daellenbach, K., Krechmer, J. E., Flaud, P. M., Worsnop,
904 D., Kulmala, M., Villenave, E., Perraudin, E., Ehn, M., and Bianchi, F.: Terpenes and their oxidation
905 products in the French Landes forest: insights from Vocus PTR-TOF measurements, *Atmos. Chem.
906 Phys.*, 20, 1941-1959, 10.5194/acp-20-1941-2020, 2020.

907 Li, H., Canagaratna, M. R., Riva, M., Rantala, P., Zhang, Y., Thomas, S., Heikkinen, L., Flaud, P. M.,
908 Villenave, E., Perraudin, E., Worsnop, D., Kulmala, M., Ehn, M., and Bianchi, F.: Atmospheric
909 organic vapors in two European pine forests measured by a Vocus PTR-TOF: insights into
910 monoterpene and sesquiterpene oxidation processes, *Atmos. Chem. Phys.*, 21, 4123-4147,
911 10.5194/acp-21-4123-2021, 2021a.

912 Li, X. B., Yuan, B., Wang, S., Wang, C., Lan, J., Liu, Z., Song, Y., He, X., Huangfu, Y., Pei, C., Cheng,
913 P., Yang, S., Qi, J., Wu, C., Huang, S., You, Y., Chang, M., Zheng, H., Yang, W., Wang, X., and

914 Shao, M.: Variations and sources of volatile organic compounds (VOCs) in urban region: insights
915 from measurements on a tall tower, *Atmos. Chem. Phys.*, 22, 10567-10587, 10.5194/acp-22-10567-
916 2022, 2022.

917 Li, Y., Zhao, J., Wang, Y., Seinfeld, J. H., and Zhang, R.: Multigeneration Production of Secondary
918 Organic Aerosol from Toluene Photooxidation, *Environ. Sci. Technol.*, 55, 8592-8603,
919 10.1021/acs.est.1c02026, 2021b.

920 Luo, H., Guo, Y., Shen, H., Huang, D. D., Zhang, Y., and Zhao, D.: Effect of relative humidity on the
921 molecular composition of secondary organic aerosols from α -pinene ozonolysis, *Environ. Sci.:*
922 *Atmos.*, 10.1039/D3EA00149K, 2024.

923 Mermet, K., Perraudin, E., Dusanter, S., Sauvage, S., Léonardis, T., Flaud, P.-M., Bsaibes, S., Kammer,
924 J., Michoud, V., Gratien, A., Cirtog, M., Al Ajami, M., Truong, F., Batut, S., Hecquet, C., Doussin,
925 J.-F., Schoemaeker, C., Gros, V., Locoge, N., and Villenave, E.: Atmospheric reactivity of biogenic
926 volatile organic compounds in a maritime pine forest during the LANDEX episode 1 field campaign,
927 *Sci. Total Environ.*, 756, 144129, <https://doi.org/10.1016/j.scitotenv.2020.144129>, 2021.

928 Mohr, C., Lopez-Hilfiker, F. D., Yli-Juuti, T., Heitto, A., Lutz, A., Hallquist, M., D'Ambro, E. L.,
929 Rissanen, M. P., Hao, L., Schobesberger, S., Kulmala, M., Mauldin III, R. L., Makkonen, U., Sipilä,
930 M., Petäjä, T., and Thornton, J. A.: Ambient observations of dimers from terpene oxidation in the
931 gas phase: Implications for new particle formation and growth, *Geophys. Res. Lett.*, 44, 2958-2966,
932 <https://doi.org/10.1002/2017GL072718>, 2017.

933 Muller, M., Eicher, P., D'Anna, B., Tan, W., and Wisthaler, A.: Direct Sampling and Analysis of
934 Atmospheric Particulate Organic Matter by Proton-Transfer-Reaction Mass Spectrometry, *Anal.*
935 *Chem.*, 89, 10889-10897, 10.1021/acs.analchem.7b02582, 2017.

936 Müller, M., Eichler, P., D'Anna, B., Tan, W., and Wisthaler, A.: Direct Sampling and Analysis of
937 Atmospheric Particulate Organic Matter by Proton-Transfer-Reaction Mass Spectrometry, *Anal.*
938 *Chem.*, 89, 10889-10897, 10.1021/acs.analchem.7b02582, 2017.

939 Ng, N. L., Canagaratna, M. R., Jimenez, J. L., Chhabra, P. S., Seinfeld, J. H., and Worsnop, D. R.:
940 Changes in organic aerosol composition with aging inferred from aerosol mass spectra, *Atmos.*
941 *Chem. Phys.*, 11, 6465-6474, 10.5194/acp-11-6465-2011, 2011.

942 Ng, N. L., Canagaratna, M. R., Zhang, Q., Jimenez, J. L., Tian, J., Ulbrich, I. M., Kroll, J. H., Docherty,
943 K. S., Chhabra, P. S., Bahreini, R., Murphy, S. M., Seinfeld, J. H., Hildebrandt, L., Donahue, N. M.,
944 DeCarlo, P. F., Lanz, V. A., Prevot, A. S. H., Dinar, E., Rudich, Y., and Worsnop, D. R.: Organic
945 aerosol components observed in Northern Hemispheric datasets from Aerosol Mass Spectrometry,
946 *Atmos. Chem. Phys.*, 10, 4625-4641, 10.5194/acp-10-4625-2010, 2010.

947 Paatero, P. and Tapper, U.: Positive matrix factorization: A non-negative factor model with optimal
948 utilization of error estimates of data values, *Environmetrics*, 5, 111-126,
949 <https://doi.org/10.1002/env.3170050203>, 1994.

950 Pagonis, D., Sekimoto, K., and de Gouw, J.: A Library of Proton-Transfer Reactions of H₃O⁺ Ions Used
951 for Trace Gas Detection, *J. Am. Soc. Mass Spectrom.*, 30, 1330-1335, 10.1007/s13361-019-02209-
952 3, 2019.

953 Paparello, D., Soukoulis, C., Schuhfried, E., Cappellin, L., Gasperi, F., Silvestri, S., Santarelli, M., and
954 Biasioli, F.: Monitoring of volatile compound emissions during dry anaerobic digestion of the
955 Organic Fraction of Municipal Solid Waste by Proton Transfer Reaction Time-of-Flight Mass
956 Spectrometry, *Bioresour. Technol.*, 126, 254-265, <https://doi.org/10.1016/j.biortech.2012.09.033>,
957 2012.

958 Peng, Y., Wang, H., Gao, Y., Jing, S., Zhu, S., Huang, D., Hao, P., Lou, S., Cheng, T., Huang, C., and
959 Zhang, X.: Real-time measurement of phase partitioning of organic compounds using a proton-
960 transfer-reaction time-of-flight mass spectrometer coupled to a CHARON inlet, *Atmos. Meas.*
961 *Tech.*, 16, 15-28, 10.5194/amt-16-15-2023, 2023.

962 Peñuelas, J. and Staudt, M.: BVOCs and global change, *Trends Plant Sci.*, 15, 133-144, 2010.

963 Pernov, J. B., Bossi, R., Lebourgeois, T., Nøjgaard, J. K., Holzinger, R., Hjorth, J. L., and Skov, H.:
964 Atmospheric VOC measurements at a High Arctic site: characteristics and source apportionment,
965 *Atmos. Chem. Phys.*, 21, 2895-2916, 10.5194/acp-21-2895-2021, 2021.

966 Peron, A., Kaser, L., Fitzky, A. C., Graus, M., Halbwirth, H., Greiner, J., Wohlfahrt, G., Rewald, B.,
967 Sandén, H., and Karl, T.: Combined effects of ozone and drought stress on the emission of biogenic

968 volatile organic compounds from *Quercus robur* L, *Biogeosciences*, 18, 535-556, 10.5194/bg-18-
969 535-2021, 2021.

970 Piel, F., Müller, M., Winkler, K., Skytte af Sättra, J., and Wisthaler, A.: Introducing the extended
971 volatility range proton-transfer-reaction mass spectrometer (EVR PTR-MS), *Atmos. Meas. Tech.*,
972 14, 1355-1363, 10.5194/amt-14-1355-2021, 2021.

973 Rasmussen, R. A. and Went, F.: Volatile organic material of plant origin in the atmosphere, *Proc. Natl.*
974 *Acad. Sci. U.S.A.*, 53, 215-220, 1965.

975 Salazar Gómez, J. I., Lohmann, H., and Krassowski, J.: Determination of volatile organic compounds
976 from biowaste and co-fermentation biogas plants by single-sorbent adsorption, *Chemosphere*, 153,
977 48-57, <https://doi.org/10.1016/j.chemosphere.2016.02.128>, 2016.

978 Scheftelowitz, M., Becker, R., and Thrän, D.: Improved power provision from biomass: A retrospective
979 on the impacts of German energy policy, *Biomass and Bioenergy*, 111, 1-12,
980 <https://doi.org/10.1016/j.biombioe.2018.01.010>, 2018.

981 Shrivastava, M., Cappa, C. D., Fan, J., Goldstein, A. H., Guenther, A. B., Jimenez, J. L., Kuang, C.,
982 Laskin, A., Martin, S. T., Ng, N. L., Petaja, T., Pierce, J. R., Rasch, P. J., Roldin, P., Seinfeld, J. H.,
983 Shilling, J., Smith, J. N., Thornton, J. A., Volkamer, R., Wang, J., Worsnop, D. R., Zaveri, R. A.,
984 Zelenyuk, A., and Zhang, Q.: Recent advances in understanding secondary organic aerosol:
985 Implications for global climate forcing, *Rev. Geophys.*, 55, 509-559,
986 <https://doi.org/10.1002/2016RG000540>, 2017.

987 Sindelarova, K., Granier, C., Bouarar, I., Guenther, A., Tilmes, S., Stavrakou, T., Müller, J. F., Kuhn,
988 U., Stefani, P., and Knorr, W.: Global data set of biogenic VOC emissions calculated by the
989 MEGAN model over the last 30 years, *Atmos. Chem. Phys.*, 14, 9317-9341, 10.5194/acp-14-9317-
990 2014, 2014.

991 Smiatek, G. and Steinbrecher, R.: Temporal and spatial variation of forest VOC emissions in Germany
992 in the decade 1994–2003, *Atmos. Environ.*, 40, 166-177,
993 <https://doi.org/10.1016/j.atmosenv.2005.11.071>, 2006.

994 Song, J., Saathoff, H., Jiang, F., Gao, L., Zhang, H., and Leisner, T.: Sources of organic gases and aerosol
995 particles and their roles in nighttime particle growth at a rural forested site in southwest Germany,
996 *Atmos. Chem. Phys.*, 24, 6699-6717, 10.5194/acp-24-6699-2024, 2024.

997 Song, J., Saathoff, H., Gao, L., Gebhardt, R., Jiang, F., Vallon, M., Bauer, J., Norra, S., and Leisner, T.:
998 Variations of PM_{2.5} sources in the context of meteorology and seasonality at an urban street canyon
999 in Southwest Germany, *Atmos. Environ.*, 119147, <https://doi.org/10.1016/j.atmosenv.2022.119147>,
1000 2022.

1001 Surdu, M., Lamkaddam, H., Wang, D. S., Bell, D. M., Xiao, M., Lee, C. P., Li, D., Caudillo, L., Marie,
1002 G., Scholz, W., Wang, M., Lopez, B., Piedehierro, A. A., Ataei, F., Baalbaki, R., Bertozzi, B.,
1003 Bogert, P., Bresseur, Z., Dada, L., Duplissy, J., Finkenzeller, H., He, X.-C., Höhler, K., Korhonen,
1004 K., Krechmer, J. E., Lehtipalo, K., Mahfouz, N. G. A., Manninen, H. E., Marten, R., Massabò, D.,
1005 Mauldin, R., Petäjä, T., Pfeifer, J., Philippov, M., Rörup, B., Simon, M., Shen, J., Umo, N. S., Vogel,
1006 F., Weber, S. K., Zauner-Wieczorek, M., Volkamer, R., Saathoff, H., Möhler, O., Kirkby, J.,
1007 Worsnop, D. R., Kulmala, M., Stratmann, F., Hansel, A., Curtius, J., Welti, A., Riva, M., Donahue,
1008 N. M., Baltensperger, U., and El Haddad, I.: Molecular Understanding of the Enhancement in
1009 Organic Aerosol Mass at High Relative Humidity, *Environ. Sci. Technol.*, 57, 2297-2309,
1010 10.1021/acs.est.2c04587, 2023.

1011 Tani, A., Hayward, S., and Hewitt, C. N.: Measurement of monoterpenes and related compounds by
1012 proton transfer reaction-mass spectrometry (PTR-MS), *Int. J. Mass. Spectrom.*, 223-224, 561-578,
1013 [https://doi.org/10.1016/S1387-3806\(02\)00880-1](https://doi.org/10.1016/S1387-3806(02)00880-1), 2003.

1014 Teskey, R., Wertin, T., Bauweraerts, I., Ameye, M., McGuire, M. A., and Steppe, K.: Responses of tree
1015 species to heat waves and extreme heat events, *Plant Cell Environ.*, 38, 1699-1712,
1016 <https://doi.org/10.1111/pce.12417>, 2015.

1017 Tillmann, R., Hallquist, M., Jonsson, Å. M., Kiendler-Scharr, A., Saathoff, H., Iinuma, Y., and Mentel,
1018 T. F.: Influence of relative humidity and temperature on the production of pinonaldehyde and OH
1019 radicals from the ozonolysis of α -pinene, *Atmos. Chem. Phys.*, 10, 7057-7072, 10.5194/acp-
1020 10-7057-2010, 2010.

1021 Trainer, M., Williams, E. J., Parrish, D. D., Buhr, M. P., Allwine, E. J., Westberg, H. H., Fehsenfeld, F.
1022 C., and Liu, S. C.: Models and observations of the impact of natural hydrocarbons on rural ozone,
1023 *Nature*, 329, 705-707, 10.1038/329705a0, 1987.

1024 van Meeningen, Y., Schurgers, G., Rinnan, R., and Holst, T.: Isoprenoid emission response to changing
1025 light conditions of English oak, European beech and Norway spruce, *Biogeosciences*, 14, 4045-
1026 4060, 10.5194/bg-14-4045-2017, 2017.

1027 Vermeuel, M. P., Novak, G. A., Kilgour, D. B., Clafflin, M. S., Lerner, B. M., Trowbridge, A. M., Thom,
1028 J., Cleary, P. A., Desai, A. R., and Bertram, T. H.: Observations of biogenic volatile organic
1029 compounds over a mixed temperate forest during the summer to autumn transition, *Atmos. Chem.*
1030 *Phys.*, 23, 4123-4148, 10.5194/acp-23-4123-2023, 2023.

1031 Vestenius, M., Hopke, P. K., Lehtipalo, K., Petäjä, T., Hakola, H., and Hellén, H.: Assessing volatile
1032 organic compound sources in a boreal forest using positive matrix factorization (PMF), *Atmos.*
1033 *Environ.*, 259, 118503, <https://doi.org/10.1016/j.atmosenv.2021.118503>, 2021.

1034 von Hessberg, C., von Hessberg, P., Pöschl, U., Bilde, M., Nielsen, O. J., and Moortgat, G. K.:
1035 Temperature and humidity dependence of secondary organic aerosol yield from the ozonolysis of β -
1036 pinene, *Atmos. Chem. Phys.*, 9, 3583-3599, 10.5194/acp-9-3583-2009, 2009.

1037 Wang, L., Slowik, J. G., Tripathi, N., Bhattu, D., Rai, P., Kumar, V., Vats, P., Satish, R., Baltensperger,
1038 U., Ganguly, D., Rastogi, N., Sahu, L. K., Tripathi, S. N., and Prévôt, A. S. H.: Source
1039 characterization of volatile organic compounds measured by proton-transfer-reaction time-of-flight
1040 mass spectrometers in Delhi, India, *Atmos. Chem. Phys.*, 20, 9753-9770, 10.5194/acp-20-9753-
1041 2020, 2020.

1042 Weber, J., Archer-Nicholls, S., Abraham, N. L., Shin, Y. M., Griffiths, P., Grosvenor, D. P., Scott, C.
1043 E., and Archibald, A. T.: Chemistry-driven changes strongly influence climate forcing from
1044 vegetation emissions, *Nat. Commun.*, 13, 7202, 10.1038/s41467-022-34944-9, 2022.

1045 Wennberg, P. O., Bates, K. H., Crouse, J. D., Dodson, L. G., McVay, R. C., Mertens, L. A., Nguyen,
1046 T. B., Praske, E., Schwantes, R. H., Smarte, M. D., St Clair, J. M., Teng, A. P., Zhang, X., and
1047 Seinfeld, J. H.: Gas-Phase Reactions of Isoprene and Its Major Oxidation Products, *Chem. Rev.*,
1048 118, 3337-3390, 10.1021/acs.chemrev.7b00439, 2018.

1049 Wu, R., Pan, S., Li, Y., and Wang, L.: Atmospheric Oxidation Mechanism of Toluene, *J. Phys. Chem.*
1050 *A*, 118, 4533-4547, 10.1021/jp500077f, 2014.

1051 Yáñez-Serrano, A. M., Bach, A., Bartolomé-Català, D., Matthaios, V., Seco, R., Llusà, J., Filella, I.,
1052 and Peñuelas, J.: Dynamics of volatile organic compounds in a western Mediterranean oak forest,
1053 *Atmos. Environ.*, 257, 118447, <https://doi.org/10.1016/j.atmosenv.2021.118447>, 2021.

1054 Yáñez-Serrano, A. M., Bourtsoukidis, E., Alves, E. G., Bauwens, M., Stavrou, T., Llusà, J., Filella,
1055 I., Guenther, A., Williams, J., Artaxo, P., Sindelarova, K., Doubalova, J., Kesselmeier, J., and
1056 Peñuelas, J.: Amazonian biogenic volatile organic compounds under global change, *Glob. Change*
1057 *Biol.*, 26, 4722-4751, <https://doi.org/10.1111/gcb.15185>, 2020.

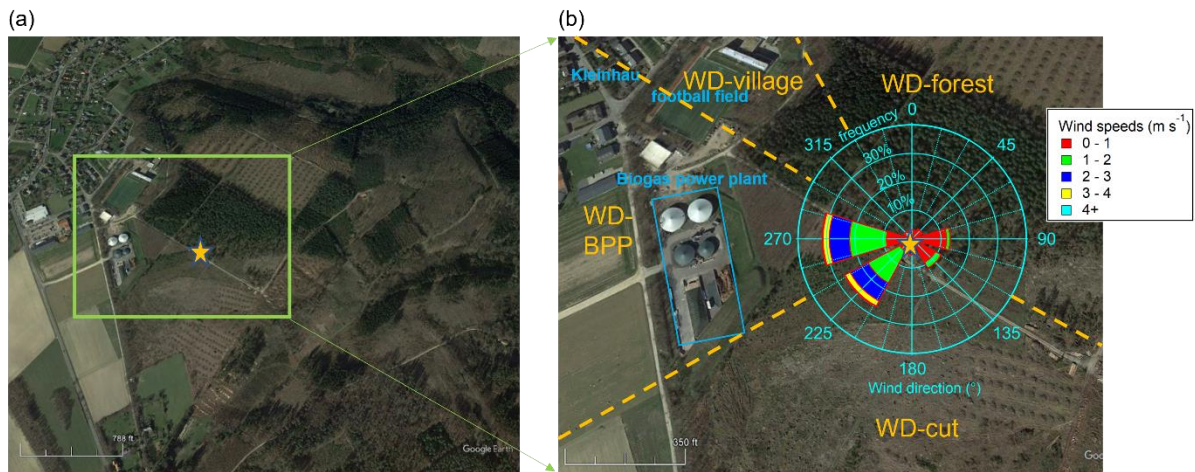
1058 Yataavelli, R. L. N., Stark, H., Thompson, S. L., Kimmel, J. R., Cubison, M. J., Day, D. A., Campuzano-
1059 Jost, P., Palm, B. B., Hodzic, A., Thornton, J. A., Jayne, J. T., Worsnop, D. R., and Jimenez, J. L.:
1060 Semicontinuous measurements of gas-particle partitioning of organic acids in a ponderosa pine
1061 forest using a MOVI-HRToF-CIMS, *Atmos. Chem. Phys.*, 14, 1527-1546, 10.5194/acp-14-1527-
1062 2014, 2014.

1063 Zaytsev, A., Koss, A. R., Breitenlechner, M., Krechmer, J. E., Nihill, K. J., Lim, C. Y., Rowe, J. C.,
1064 Cox, J. L., Moss, J., Roscioli, J. R., Canagaratna, M. R., Worsnop, D. R., Kroll, J. H., and Keutsch,
1065 F. N.: Mechanistic study of the formation of ring-retaining and ring-opening products from the
1066 oxidation of aromatic compounds under urban atmospheric conditions, *Atmos. Chem. Phys.*, 19,
1067 15117-15129, 10.5194/acp-19-15117-2019, 2019.

1068 Zhang, X., McVay, R. C., Huang, D. D., Dalleska, N. F., Aumont, B., Flagan, R. C., and Seinfeld, J. H.:
1069 Formation and evolution of molecular products in β -pinene secondary organic aerosol, *Proc.*
1070 *Natl. Acad. Sci. U.S.A.*, 112, 14168-14173, doi:10.1073/pnas.1517742112, 2015.

1071

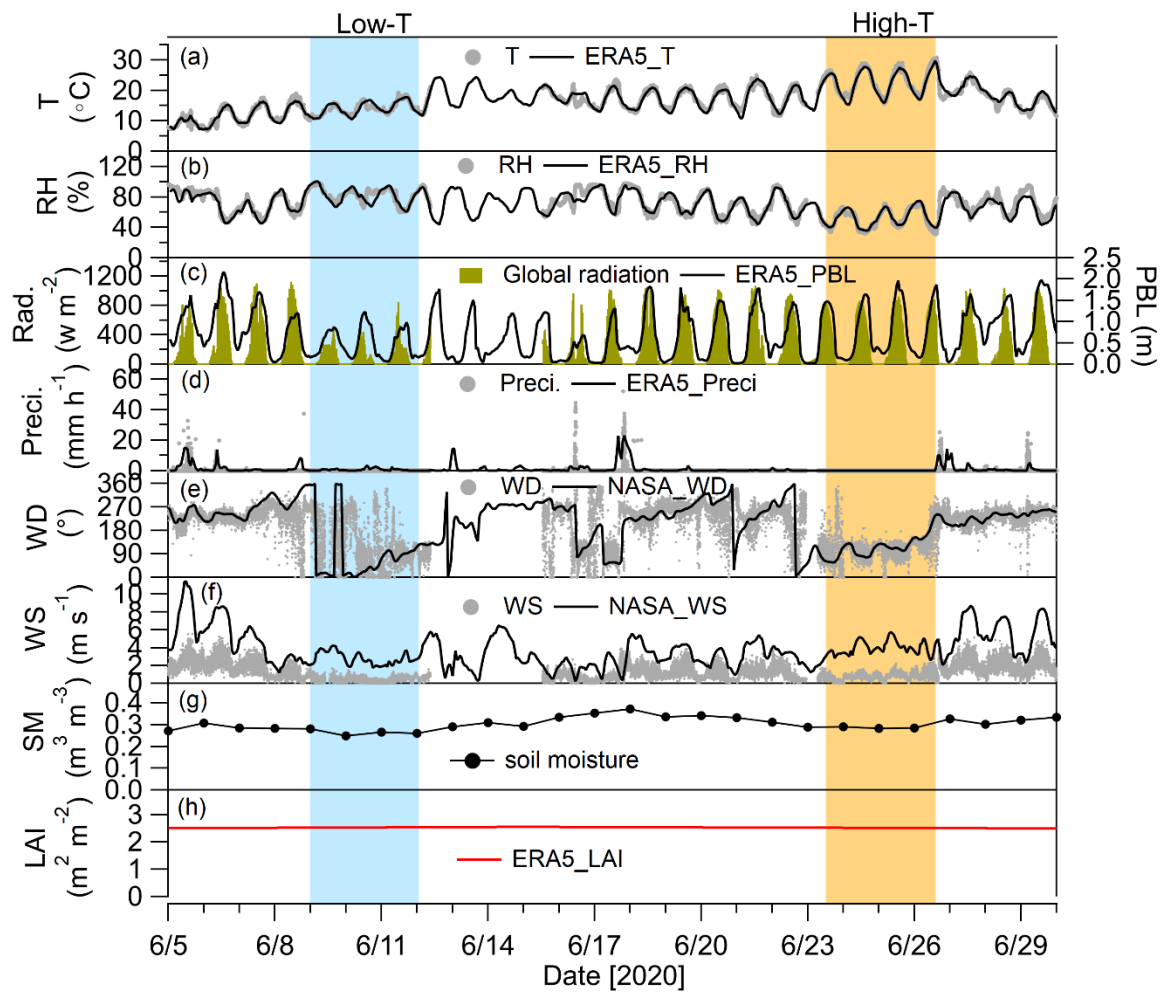
1072



1073

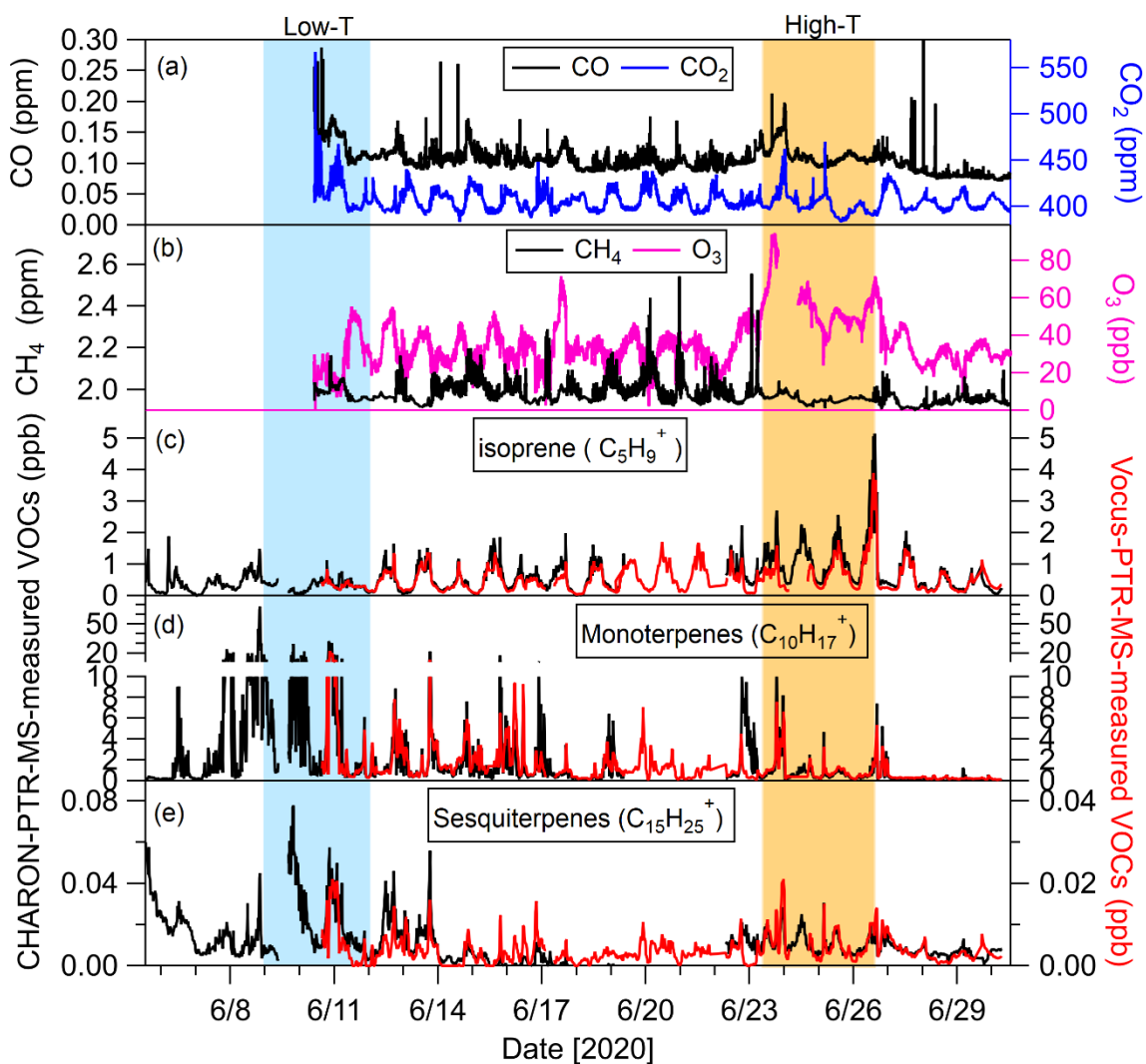
1074 **Figure 1.** (a) Location of the sampling site (orange star) (©Google Earth); (b) a close look at
 1075 sampling site with the centered wind rose for the entire measurement period. The orange dash
 1076 lines are shown for distinguishing different sectors of wind direction (WD). The WD-forest of
 1077 0-120° is influenced by an intact forest area, the WD-cut of 120-240° is influenced by a clear-
 1078 cut area, the WD-BPP of 240-300° is influenced by a biogas power plant (blue rectangle) and
 1079 the WD-village of 300-330° is influenced by the residential areas of Kleinhaus.

1080



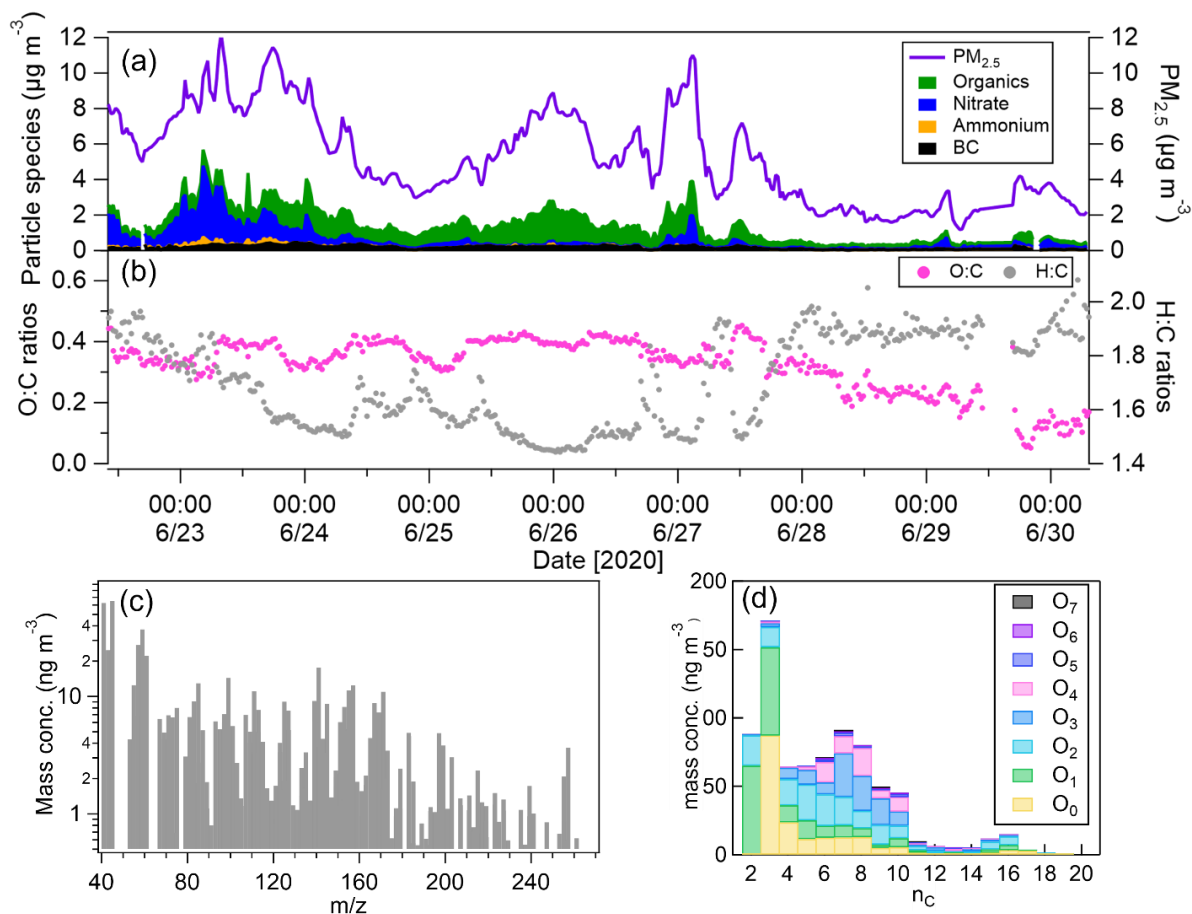
1081

1082 **Figure 2.** (a-f) Time series of meteorological data measured at the sampling site with hourly
 1083 data of temperature (T), relative humidity (RH), precipitation (Preci.) and planetary boundary
 1084 layer (PBL) height obtained from ERA5 reanalysis (Hersbach et al., 2020) and hourly data of
 1085 wind direction and speed (WD and WS) obtained from NASA Power Data Access Viewer
 1086 (power.larc.nasa.gov); (g) daily soil moisture (SM) measured by a cosmic ray neutron sensor
 1087 which was located ~ 150 m southwest of the sampling site; and (h) leaf area index (LAI)
 1088 obtained from ERA5 reanalysis. The blue and yellow shaded areas mark the low-T and high-T
 1089 episodes.



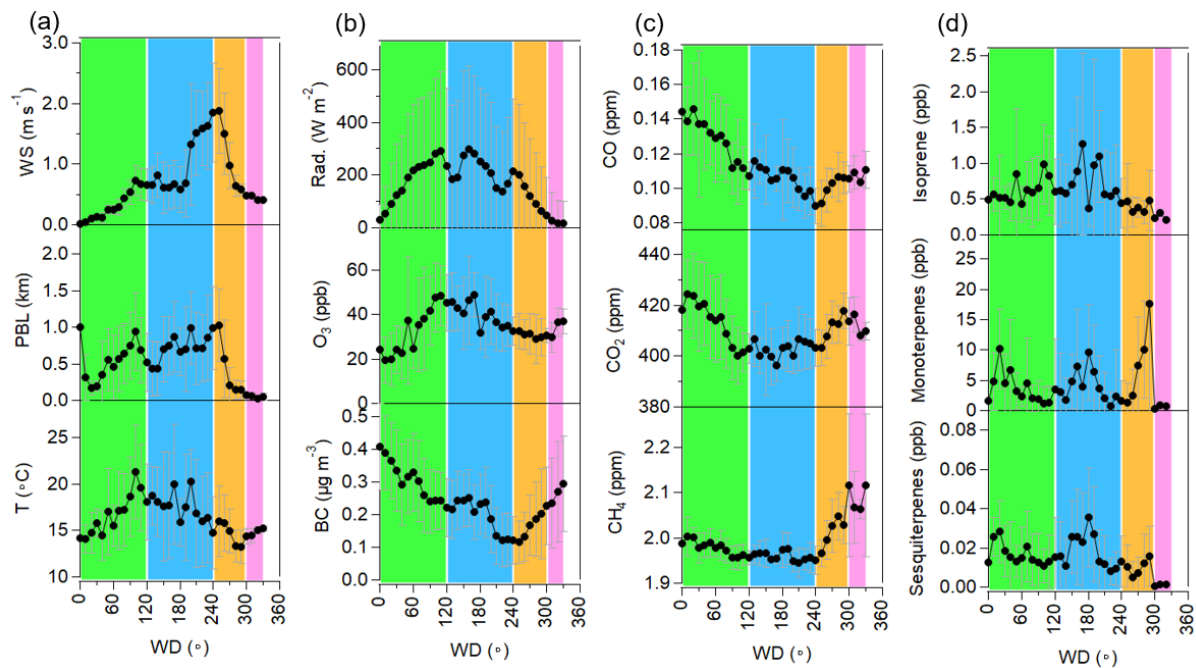
1090

1091 **Figure 3.** Time series of gas species: (a) CO and CO₂; (b) CH₄ and O₃; (c-e) isoprene,
 1092 monoterpene, sesquiterpene measured by the CHARON-PTR-ToF-MS (black lines) and
 1093 Vocus-PTR-ToF-MS (red lines) respectively. The blue and yellow shaded areas mark the low-
 1094 T and high-T episodes.



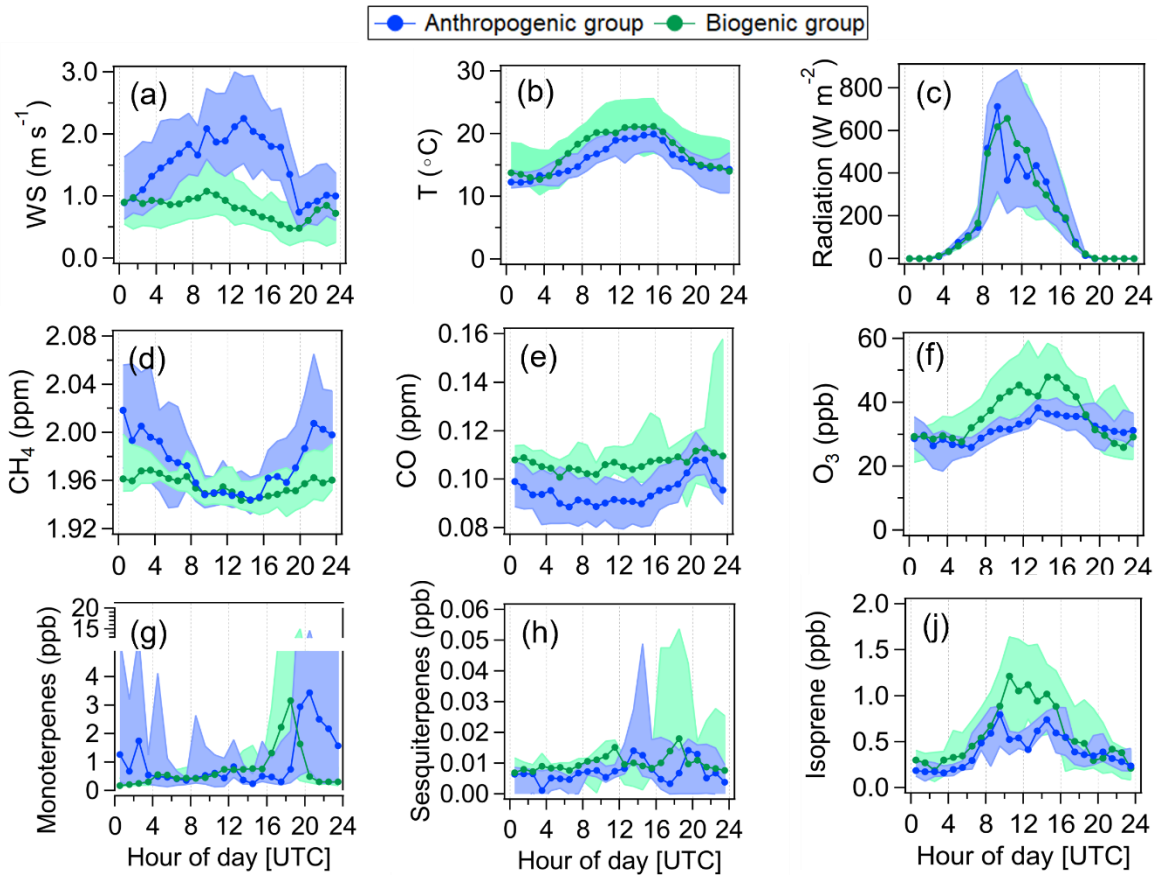
1095

1096 **Figure 4.** Time series of (a) mass concentrations of $PM_{2.5}$, BC and semi-volatile particle species
 1097 (organics, nitrate and ammonium) measured by the CHARON-PTR-ToF-MS simultaneously
 1098 available during 22nd-30th June; (b) oxygen to carbon (O:C) and hydrogen to carbon (H:C) ratios
 1099 of organics. (c) average mass spectrum of organics; (d) mass distributions of organics associated
 1100 with $C_xH_yO_{0-7}^+$ resolved by the carbon and oxygen numbers (n_C and n_O).



1101

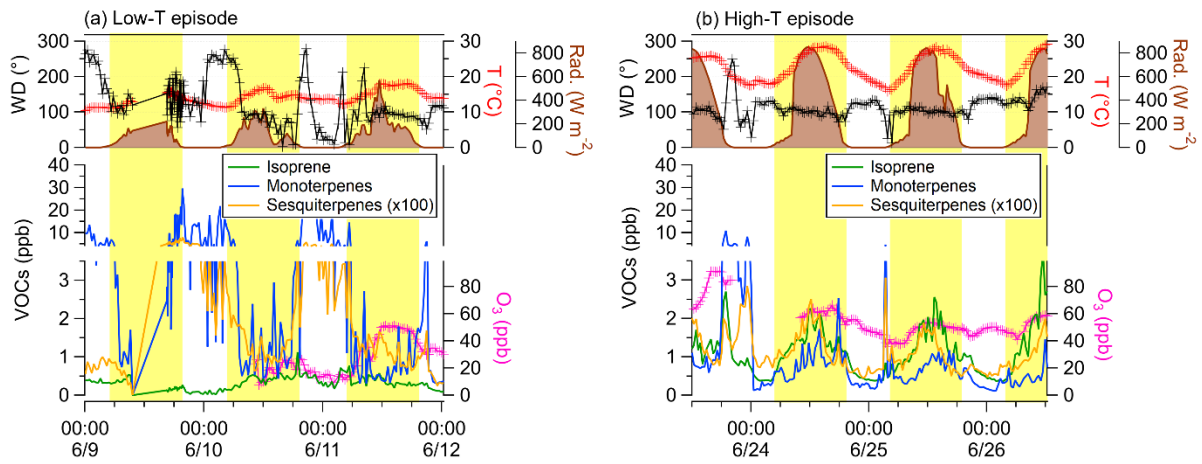
1102 **Figure 5.** Variations of (a) wind speed (WS), planetary boundary layer (PBL) and ambient
 1103 temperature; (b) global radiation, O₃ and BC mass concentrations; (c) mixing ratios of CO, CO₂
 1104 and CH₄ and (d) mixing ratios of isoprene, monoterpenes and sesquiterpenes as a function of
 1105 wind direction (WD). The black dots and whiskers represent the mean values and standard
 1106 deviations in each WD bin of 10°. Data within the WD1 of 0-120° is influenced by an intact
 1107 forest area (light green), the WD2 of 120-240° is influenced by a clear-cut area (light blue), the
 1108 WD3 of 240-300° is influenced by a biogas power plant (yellow) and the WD4 of 300-330° is
 1109 influenced by the village (pink).



1110

1111 **Figure 6.** Diurnal variations of (a-c) wind speeds, ambient temperature and global radiation;
 1112 (d-f) CH₄, CO and O₃; (g-j) monoterpenes, sesquiterpenes and isoprene. The blue and green
 1113 markers represent the median values for the anthropogenic-group and biogenic-group, which
 1114 were calculated from the data within the sectors of WD-forest and WD-cut, and WD-BPP and
 1115 WD-village, respectively. The shaded areas represent the 25th and 75th percentiles.

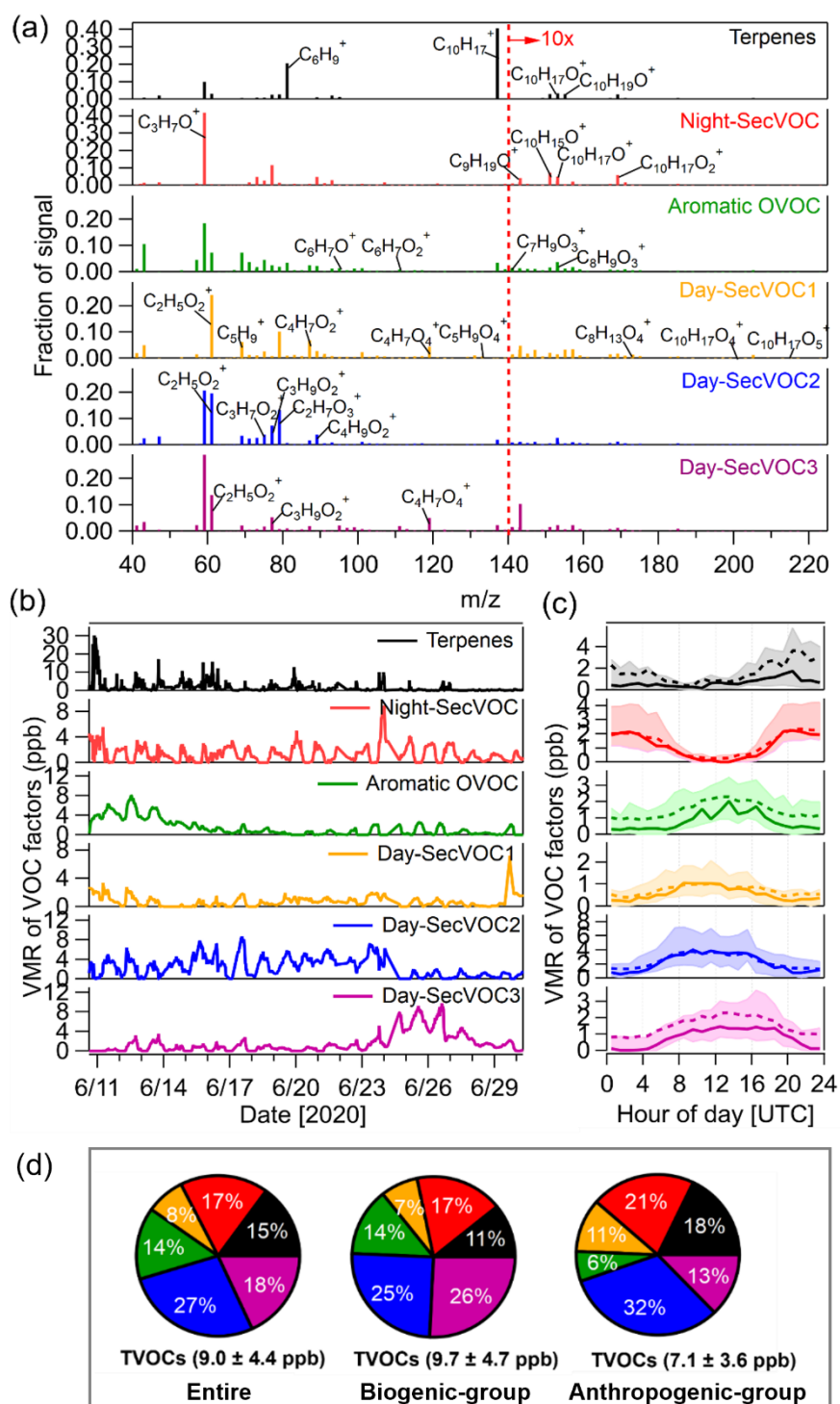
1116



1117

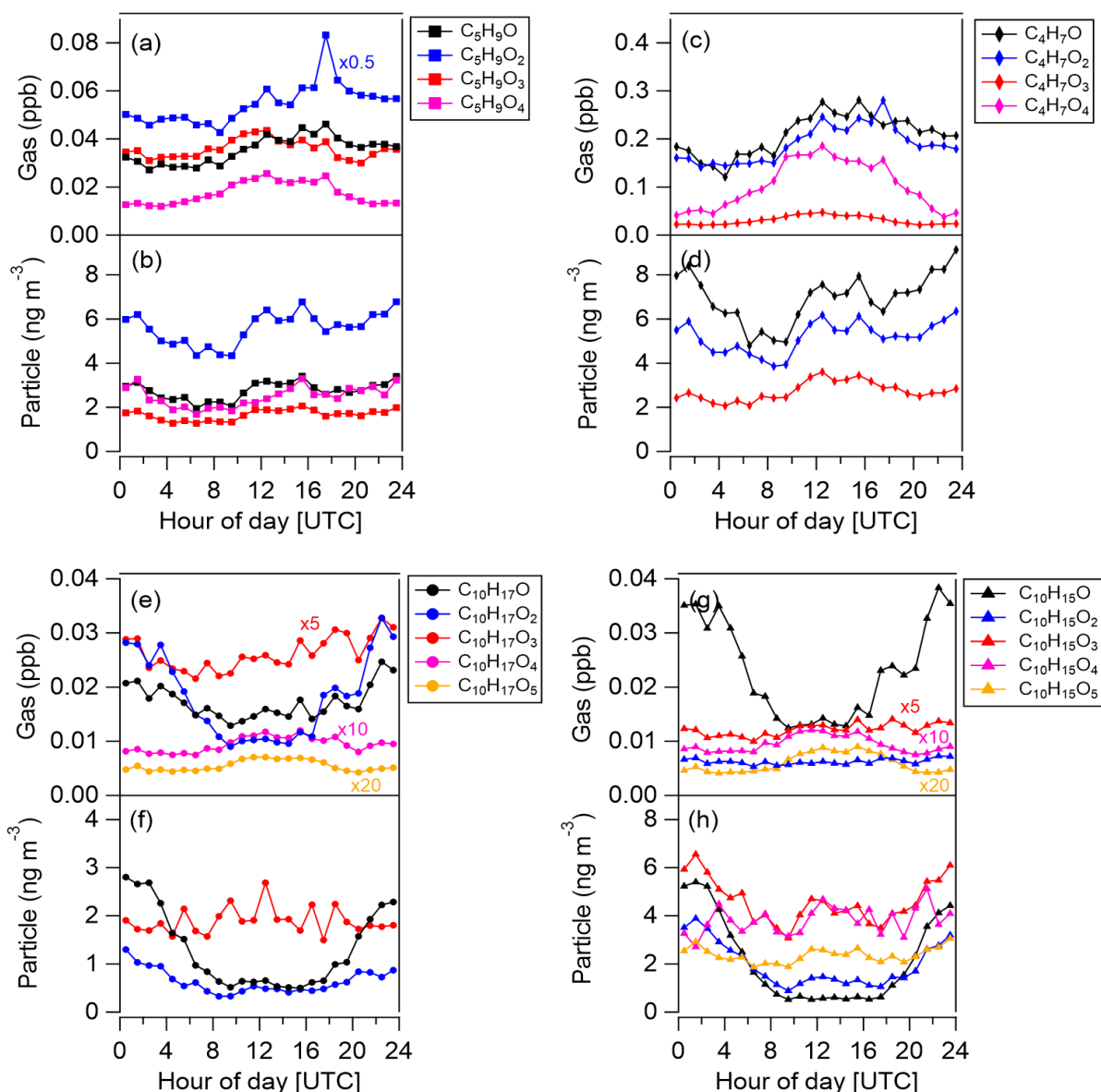
1118 **Figure 7.** Time series of wind direction, ambient temperature, global radiation, isoprene,
1119 monoterpenes, sesquiterpenes and O₃ during the low-T episode (a) and high-T episode (b). The
1120 yellow shaded areas mark the daytime from 4:00-20:00 UTC.

1121



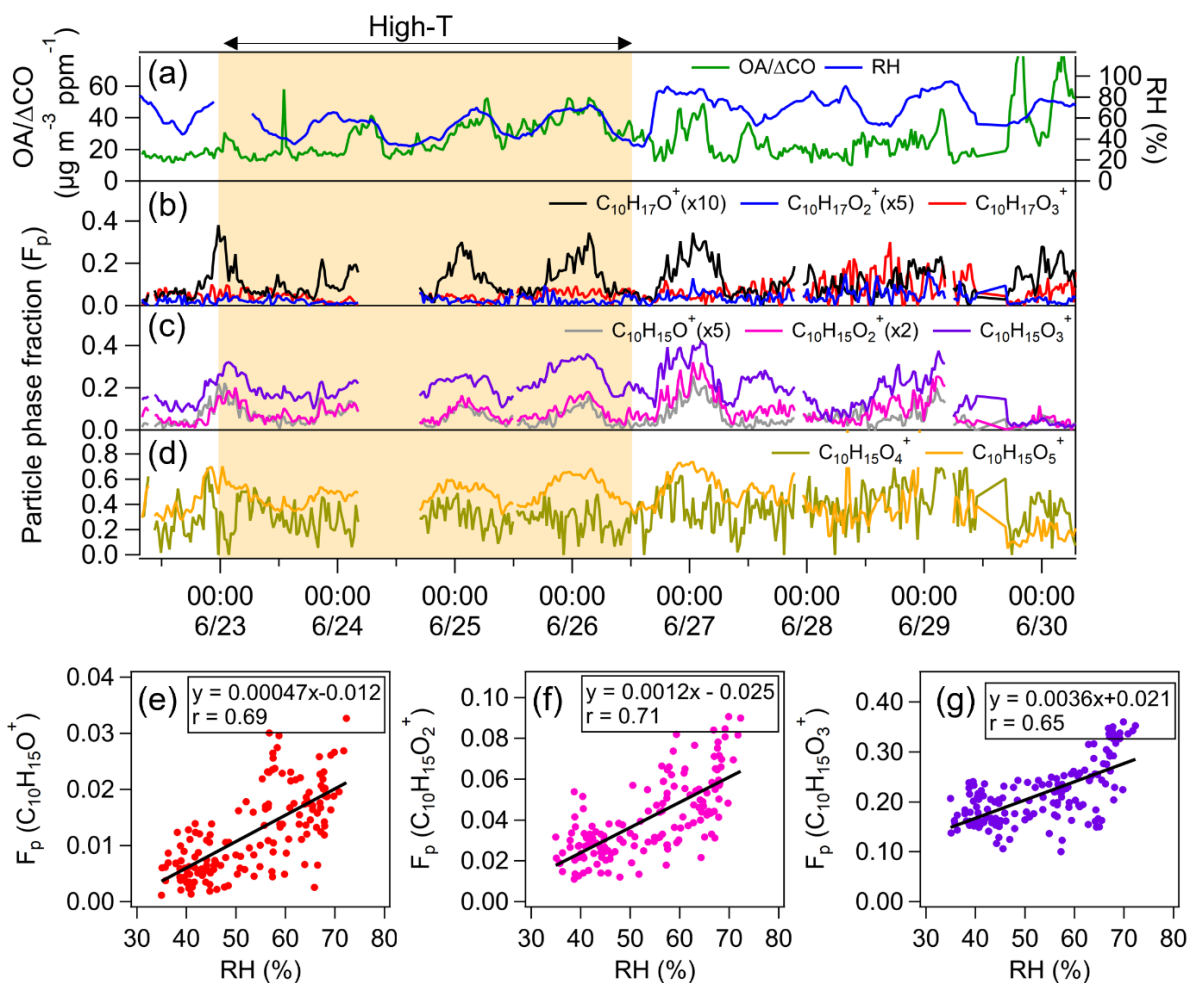
1122

1123 **Figure 8.** (a) Factor profiles of six VOC factors resolved from the PMF analysis of Vocus-PTR-
 1124 ToF-MS data. The fraction of signal at high mass range (m/z 140-230) is scaled by a factor of
 1125 10; (b) time series of six VOC factors; (c) diurnal variations of six VOC factors during the entire
 1126 measurement campaign. The solid and dash lines represent median and mean values
 1127 respectively and the shaded areas represent the 25th and 75th percentiles. (d) Average
 1128 contributions of six VOC factors to TVOCs for the entire measurement campaign and the
 1129 biogenic-group and anthropogenic-group.



1130

1131 **Figure 9.** Diurnal variations of (a-d) isoprene oxidation products ($C_5H_9O_{1-4}^+$ and $C_4H_7O_{1-4}^+$) in
 1132 gas and particle phases; (e-h) monoterpene oxidation products ($C_{10}H_{17}O_{1-5}^+$ and $C_{10}H_{15}O_{1-5}^+$) in
 1133 gas and particle phases calculated for the measurement period of 22nd-30th of June. Gas- and
 1134 particle-phase data were taken from the Vocus-PTR-ToF-MS and CHARON-PTR-ToF-MS
 1135 measurements, respectively. The higher-oxidized particle-phase products from isoprene
 1136 ($C_4H_7O_4^+$) and monoterpenes ($C_{10}H_{17}O_{4-5}^+$) cannot be detected by the CHARON-PTR-ToF-
 1137 MS.



1138

1139 **Figure 10.** Time series of (a) OA/ΔCO and relative humidity (RH); (b-d) particle phase fraction
 1140 of monoterpene oxidation products (C₁₀H₁₇O₁₋₃⁺ and C₁₀H₁₅O₁₋₅⁺) from 22nd-30th of June. The
 1141 yellow shaded area marks the high-T episode. (e-f) Correlations of the time series of particle
 1142 phase fraction of C₁₀H₁₅O₁₋₃⁺ with RH during high-T episode.